Biol Cybern (2013) 107:179–200
DOI 10.1007/s00422-012-0545-z

ORIGINAL PAPER

Biological Cybernetics

Instantaneous kinematic phase reflects neuromechanical response to lateral perturbations of running cockroaches

Shai Revzen · Samuel A. Burden · Talia Y. Moore · Jean-Michel Mongeau · Robert J. Full

Received: 19 July 2012 / Accepted: 27 December 2012 / Published online: 1 February 2013
© Springer-Verlag Berlin Heidelberg 2013

Abstract Instantaneous kinematic phase calculation allows the development of reduced-order oscillator models useful in generating hypotheses of neuromechanical control. When perturbed, changes in instantaneous kinematic phase and frequency of rhythmic movements can provide details of movement and evidence for neural feedback to a system-level neural oscillator with a time resolution not possible with traditional approaches. We elicited an escape response in cockroaches (*Blaberus discoidalis*) that ran onto a movable cart accelerated laterally with respect to the animals' motion causing a perturbation. The specific impulse imposed on animals (0.50 ± 0.04 m s^{-1}; mean, SD) was nearly twice their forward speed (0.25 ± 0.06 m s^{-1}). Instantaneous residual phase computed from kinematic phase remained constant for 110 ms after the onset of perturbation, but then decreased representing a decrease in stride frequency. Results from direct muscle action potential recordings supported kinematic phase results in showing that recovery begins with self-stabilizing mechanical feedback followed by neural feedback to an abstracted neural oscillator or central pattern generator. Trials fell into two classes of forward velocity changes, while exhibiting statistically indistinguishable frequency changes. Animals pulled away from the side with front and hind legs of the tripod in stance recovered heading within 300 ms, whereas animals that only had a middle leg of the tripod resisting the pull did not recover within this period. Animals with eight or more legs might be more robust to lateral perturbations than hexapods.

Keywords Biomechanics · Phase · Neuromechanical control · Neural clock · Locomotion · Cockroach · Perturbation

S. Revzen · T. Y. Moore · R. J. Full (✉)
Department of Integrative Biology, University of California, Berkeley, CA 94720, USA
e-mail: rjfull@berkeley.edu

S. A. Burden
Department of Electrical Engineering and Computer Sciences, University of California, Berkeley, CA 94720, USA

J.-M. Mongeau
Biophysics Graduate Group, University of California, Berkeley, CA 94720, USA

Abbreviations

Axes	Y-axis is positive along the line of platform translation. Also called lateral axis. Z-axis is perpendicular to the Y-axis, positive vertical of the platform. X-axis is perpendicular to both the Y- and Z-axes, and positive in the direction of cockroach locomotion. Also called the forward axis
Vx	Component of cockroach velocity in trackway direction
Vy	Component of cockroach velocity across trackway
COM	Center of mass
CPG	Central pattern generator
EMG	Electromyography
IBI	Inter-burst interval. The time between two bursts of muscle action potentials in an electromyography
ISI	Inter-spike interval
LLS	Lateral leg spring model
MAP	Muscle action potential
PCA	Principal component analysis
LLS	Lateral leg spring model

AEP	Anterior extreme position. The transition from swing to stance.
PEP	Posterior extreme position. The transition from stance to swing.
SLIP	Spring loaded inverted pendulum model

List of symbols

Φ	Phase threshold between classes (one class has $\Phi - \pi < \phi_0 < \Phi$, the other $\Phi < \phi_0 < \Phi + \pi$)
ϕ_0	Predictor phase
ϕ, θ	Phases
ω	Derivative of phase with respect to time, i.e. instantaneous frequency
$\Delta\phi$	Residual phase
x, v	Position, velocity time series used to create complex phase time series
z	Complex phase time series $\langle . \rangle$ mean value; $\langle w(t) \rangle$ is the expectation of the variable $w(t)$
$t_1$pre	Starting time window pre-perturbation
$t_2$pre	Ending time window pre-perturbation
t_{step}	Step duration
t_{on}	Onset of perturbation
$t_1$post	Starting time window post-perturbation
$t_2$post	Ending time window post-perturbation
std	Standard deviation operator; std$[w(t)]$ is the standard deviation of the variable $w(t)$
exp	(Complex) exponential function
arg	Complex argument (i.e., polar angle) function
C_0	Class 0, one of the two phase classes (in red)
C_1	Class 1, one of the two phase classes (in blue)
Vx_0	Mean of cockroach velocity in trackway direction for C_0
Vx_1	Mean of cockroach velocity in trackway direction for C_1
L_1 norm	Sum of absolute differences
L_2 norm	Square root of sum of squared differences, same as root mean square (RMS) up to a scale
N	Parameter governing the number of bootstrap trials used for testing classification significance; N^2 trials for H_1 and $H_{0(a)}$ are compared with a nested bootstrap of N trials of N nested trials each.
n	Number of trials provided by an individual animal
H_1	Statistical hypothesis that classes the C_0 and C_1 obtained from ϕ_0 and Φ describe animals that behave differently.
$H_{0(a)}$	Statistical hypothesis that trial classes C_0 and C_1 are selected at random from the same distribution of animal motions.
$H_{0(b)}$	Statistical hypothesis that trial classes C_0 and C_1 are selected to be most dissimilar classes that can be obtained based on a choice of Φ, while still being selected at random from the same distribution of animal motions.
χ^2	Statistical distribution and associated test

1 Introduction

Using the rhythmic motion of diverse body structures and appendages, animals adopt a wide spectrum of locomotor behaviors to move through every variety of natural environments. As they move, animals must respond to unexpected perturbations such as changes in terrain, injury to limbs, and the behavior of predators, prey, and conspecifics. We propose that within the kinematic responses to these perturbations reside patterns revealing the interplay between neural and mechanical stabilization that govern the recovery from perturbation. Using the instantaneous phase and frequency of rhythmic limb movements, Revzen et al. [2008] offer a general framework for identifying which candidate feedback pathways within neuromechanical control architectures play the dominant role in coordinating neuromechanical oscillations (Fig. 1).

1.1 Neuromechanical control architectures

With the simplest neuromechanical control architectures possible, at least three types of feedback pathways contribute to stabilization. Figure 1A corresponds to a hypothesis based primarily on mechanical stabilization, Fig. 1B on time-invariant (classical) reflex feedback, and Fig. 1C on feedback modulation of the entire gait pattern. The overall framework of neuromechanical control in which we ground these hypotheses assumes that motions are driven by endogenously produced rhythmic pattern oscillations emitted from a CPG (Delcomyn 1980; Büschges 2005; Büschges et al. 2011; Marder et al. 2005; Grillner 1985; MacKay-Lyons 2002). For the running behavior described here, we use CPG to represent a reduced-order, system-level model composed of multiple interacting neural CPG circuits that are phase-locked (Revzen et al. 2008; Revzen 2009; Fuchs et al. 2011, 2012). The CPG is coupled to an oscillating mechanical system composed of appendages, skeleton and the muscles that connect them. In turn, this mechanical system is coupled to the environment.

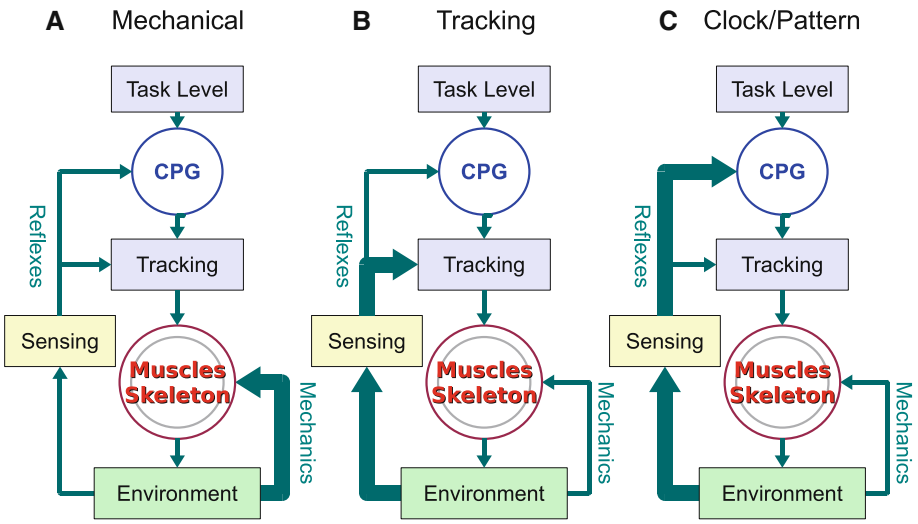

Fig. 1 Three types of feedback in a neuromechanical control architectures (Revzen et al. 2008). The "Task Level" control block represented descending neural signals and physiological state. We assumed its outputs to be held constant throughout a behavior. A central pattern generator (CPG, *blue circle*) contained the self-exciting neural circuitry that generated the rhythmic pattern for the behavior. Here CPG represents an abstracted, reduced-order model of a neural oscillator, where one or more interacting neural CPG circuits are phase-locked, and not any identified neural circuits. All reflex-based neural modulation of the CPG signal lay in the "Tracking" blocks. Tracking contained no persistent state and was not self-exciting. The "Muscles and Skeleton" (*nested circles*) contained the mechanical state of the body, which is subject to manipulation by forces from the environment. The body interacted mechanically with the "Environment" block and also modified the representation of the environment returned by the "Sensing" block. Information flow is indicated by arrows. We considered three forms of feedback (*thick arrows*): **A** mechanical feedback, wherein muscle activation remains unchanged and recovery from perturbation is mediated by properties of the mechanical interaction with the environment; **B** tracking feedback, wherein recovery is the result of reflexes bringing the motions of the body into line with the reference motions indicated by the pattern produced from the CPG; **C** clock or pattern feedback, wherein feedback changes the pattern of activation produced by the CPG

At the most rapid speeds, mechanical systems dominate control because they provide an immediate response to perturbations (Fig. 1A), whereas neural feedback may be limited by signaling bandwidth, computation ability, and the delays inherent in muscle force recruitment. When a mechanical system is tuned to its environment, mechanical feedback can be remarkably effective. (Kubow and Full 1999) showed that when biologically realistic ground reaction forces are simulated, a hexapedal morphology could mechanically self-stabilize. This discovery was corroborated by finding that running cockroaches begin to recover from a lateral impulse within 14 ms—a response time that challenges the fastest of reflexes (Ahn and Full 2002), and would barely provide sufficient time for neural feedback from their tibial campaniform sensilla (Ridgel et al. 2001) or allow for force development even if triggered from more rapidly activated femur and coxa sensillae as in locust. Muscle action potentials of a set of putative control muscles show no difference between running on rough terrain and on flat ground. Neither circumoesophageal lesion (disconnecting the brain from the thoracic nerve cord; removal of the arrow from "Task Level" to "CPG" in Fig. 1) nor distal leg denervation (removal of that part of environmental feedback that is sensed via the leg itself in the arrow from "Environment" to "Sensing" in Fig. 1) prevent rapid running in cockroaches (Ridgel and Ritzmann 2005; Noah et al. 2004). Spiders and cockroaches show no change in the limb kinematics when running rapidly over a mesh that removes ninety percent of the ground contact area (Spagna et al. 2007). Instead of relying on precise stepping informed by neural feedback, these arthropods use mechanical feedback distributed along their legs and enhanced by the passive mechanics of leg hairs.

There is a sound theoretical basis supporting mechanical self-stabilization in running. Mathematical analysis of models of running show self-stabilization in both the Spring Loaded Inverted Pendulum (SLIP) model (Ghigliazza et al. 2005; Altendorfer et al. 2004; Seyfarth et al. 2003) that governs sagittal plane running dynamics and the Lateral Leg Spring (LLS) model (Schmitt and Holmes 2000a, b) that describes horizontal running in sprawl-postured animals. The simple LLS model of the cockroach and other more morphologically grounded models exhibit robust stability to lateral impulse perturbations, despite using little or no sensory feedback (Schmitt and Holmes 2001, 2003; Schmitt et al. 2002; Kukillaya and Holmes 2009; Proctor and Holmes 2008). Proprioceptive neural feedback, if present, can assist the feedfoward preflexive dynamics (Proctor and Holmes 2010). More representative models that include legs with joints, antagonistic Hill-type muscle models and proprioceptive neural feedback (Kukillaya and Holmes 2009; Kukillaya et al. 2009) reveal behavior similar to the simpler models after phase-reduction (Proctor et al. 2010). Taken together,

the combination of theoretical plausibility and empirical evidence provides a strong case for mechanical self-stabilization during high-speed running (Holmes et al. 2006).

At slower speeds and for more precise movements, neural feedback from sensors (Fig. 1B) is the dominant modality of control. The important role of neural reflexes in slow locomotion is well established in insects. For the slow, quasi-static locomotion of stick insects, the artificial neural net "WalkNet" provides an effective representation of control (Cruse and Schwarze 1988; Cruse and Knauth 1989; Cruse et al. 2007; Schilling et al. 2007) that includes targeted foot placement mediated by feedback. The model is largely kinematic in nature because inertia and momentum play almost no role in slow walking (Klavins et al. 2002). Even in slow running insects, sensors associated with neural reflexes respond to environmental perturbations by feeding back on the patterns emitted by a CPG (Ijspeert 2008; Ritzmann and Büschges 2007; Fig. 1B symbolized by the "Tracking" block).

A large body of research has shown that the neural reflexes controlling locomotion are far richer in behavior than our typical view of a stereotyped, negative feedback loop (e.g., Pearson 1995, 2004). For example, load compensating reactions in land mammals and arthropods depend on the type of sensor (sensing self vs. environment), the preparation studied (intact vs. isolated), the task (immobile, walking vs. running), the intensity of muscle contraction, the phase in the gait (swing vs. stance), and the relative importance of passive versus reflexive stiffness (Duysens et al. 2000; Zehr and Stein 1999). Some mammalian reflexes that provide negative force feedback gains under most circumstances provide positive gains during locomotion, increasing force production during stance (Prochazka et al. 1997a, b; Pearson and Collins 1993). Sensory information may introduce coordination and adaptation of locomotor patterns that would otherwise be independent and unmodulated (Grillner and Wallén 2002), or it may be critically necessary for oscillations to appear at all (Pearson 1993, 1995, 2004).

We place locomotor neural reflexes regardless of whether they were triggered by proprioceptive or exteroceptive sensing into two broad categories—one that affects the output of the CPG (Tracking; Fig. 1B) and the other that alters the rhythm of the CPG itself (Fig. 1C). One may envision tracking feedback to be a means of matching a limb's motion to an implied reference motion generated by the CPG and can be characterized as following an equilibrium-point trajectory (Jaric and Latash 2000). Mathematically, tracking is time-invariant, stateless (has no memory of past inputs), and functions by comparing the actual state of the body to the reference provided by the CPG, then generating force activation in muscles. Tracking contains no persistent state and is not self-exciting. Feedback via such tracking reflexes (Fig. 1B) does not modulate the rhythm emitted by the CPG. In the Fig. 1C category, we define neural feedback that does alter the rhythm from the CPG. Neural feedback in this category could result in changes in the frequency output by the CPG.

1.2 Kinematic phase can reflect feedback to the systems-level CPG

In Revzen et al. [2008], we proposed methods for identifying the interplay of neural and mechanical feedback by probing rhythmic behaviors through computing phase estimates derived from kinematic observations—a "kinematic phase". Examination of kinematic phase can illuminate the coupling between the mechanical oscillator—the body, muscle, and skeleton—and the neural oscillator(s) (CPG(s)) that drives it (Fig. 1). When an animal is engaged in a rhythmic behavior, all the subsystems involved in producing that behavior and all observable quantities describing those subsystems will oscillate rhythmically. The implication for experimental biomechanics is that the kinematics of the body and its subsystems must reflect the underlying oscillator state.

The advantage of the kinematic phase method (Revzen and Guckenheimer 2008) is that for animal locomotion with stable oscillations, phase provides a *quantitative and predictive* model of movement. When given the readily measured kinematic state of the animal in as little as two consecutive frames of video, one can compute the phase and frequency, extrapolate the linear relationship of phase to time, and predict the kinematic states at all future times. In practice, because animals are continuously perturbed from the idealized dynamics of the template (Full and Koditschek 1999), the accuracy of prediction diminishes over time and requires frequency estimates over more than just a pair of frames. Nevertheless, the ability to take a dataset only a fraction of a step long, obtain phase and frequency, and project anticipated kinematics several strides into the future provides a powerful means for testing perturbation recovery against an unperturbed alternative.

For constant frequency locomotion such as running, the animal's motions will over time settle to a constant phase relative to the timing of the signal emitted by the systems-level, synchronized CPG. This phenomenon is known as "phase locking" or "entrainment". We may thus postulate that the pre-perturbation animal is an entrained neural and mechanical oscillator. Relative to time, the kinematic phase of such an animal would follow a linear model with running frequency being the slope of a phase versus time plot. Due to entrainment, the kinematic phase must be at a constant phase offset relative to the phase of the systems-level CPG.

When the animal is perturbed, some transient response appears and decays, and the animal resumes running at a constant, but possibly different, frequency. We propose to detect changes in phase by fitting a linear regression model to pre-perturbation phase data and extrapolating an expected phase

past the perturbation and into the recovery phase. Subtracting that estimate from the post-perturbation kinematic phase, we will provide a "residual phase" succinctly expressing any changes in the animal's rhythm and timing of movement.

Figure 2A–D, derived from (Revzen et al. 2008), shows the procedure of going from leg kinematics to residual phase using experimental data from a hexapedal runner experiencing a perturbation. The position data represent the fore-aft leg motions relative to the body as a function of time. Theoretically possible outcomes of the perturbation experiment are represented with simulated data in Fig. 2E–G. In Fig. 2F, we show the linear model extrapolations for position and residual phase post-perturbation (i.e., gray lines). Differences in the slope of the linear models (Fig. 2G) indicate changes in running frequency, and can only persist if the neural signal driving the muscles changes frequency as well. Thus, if we see no residual phase change after a perturbation (Fig. 2E), we hypothesize that the most parsimonious neural control architecture characterizing the response is one that involves mechanical feedback (Fig. 1A). If the perturbation causes a change in the systems-level CPG frequency, as seen in Fig. 2G, we reject the possibility of the mechanical feedback pathway (Fig. 1A) and the tracking neural feedback pathway (Fig. 1B) in favor of the control architecture sending neural feedback to the systems-level CPG (Fig. 1C). Phase change outcomes (Fig. 2F) can appear in all three feedback architectures (Fig. 1), but can be further analyzed based on their sensitivity to perturbation magnitudes.

1.3 Model system testing the utility of kinematic phase

The best candidates to test neuromechanical control hypotheses using kinematic phase are animals whose anchored morphology expresses the rhythmic motions of the template with many easily measurable appendages. These animals would expose a great deal of phase information through their kinematics, making kinematic phase a reliable estimate of their overall phase. Here, we test these hypotheses using a hexapedal runner, the cockroach *Blaberus discoidalis*, not only because of the phase data offered by six oscillating legs, but because few species have as extensive a biomechanical (Kram et al. 1997; Full et al. 1991; Full and Tu 1990; Ting et al. 1994; Jindrich and Full 1999; Ahn et al. 2006; Ahn and Full 2002) and neurophysiological (Watson and Ritzmann 1998a, b; Watson et al. 2002a, b; Zill et al. 1981, 2004, 2009) characterization.

In this study, we used kinematic phase (Revzen and Guckenheimer 2008) to investigate the time-course of cockroach recovery from a lateral impulse perturbation. The perturbations occurred when the animals were running at intermediate speeds, where the likelihood of viewing the interplay between neural and mechanical feedback was the greatest. By comparing instantaneous residual phase before and after the perturbation (Fig. 2), we could propose when mechanical feedback was sufficient, neural feedback must be used, or a sensory signal was sent to modulate the abstracted, systems-level CPG (Fig. 1). Because we measured leg kinematics, we could explore the relationship of an animal's posture and its mechanical response to its control strategy.

To test whether instantaneous kinematic phase at the systems level reflects neuromechanical feedback in well-studied leg control muscles (Sponberg et al. 2011a, b, Sponberg and Full 2008; Ahn and Full 2002; Ahn et al. 2006; Full et al. 1998), we recorded muscle action potentials (MAPs) from femoral extensors 178 and 179. We selected these muscles because their single fast motor neuron innervation (D_f) allows the simplest possible characterization of activation (Pearson and Iles 1971). Moreover, Sponberg and Full [2008] found no significant difference in the inter-spike interval, burst phase or inter-burst period between flat and very rough terrain suggesting a greater contribution of mechanical feedback. By contrast, during the largest perturbations, neural feedback was detectable as a phase shift of the central rhythm. In this key control muscle, we hypothesize that the lack of change in instantaneous kinematic phase will be associated with no change in MAP inter-burst periods, supporting a possible greater reliance on mechanical feedback, whereas a change in kinematic phase will coincide with a concomitant change in MAP inter-burst periods reflecting neural feedback

2 Lateral perturbation experiment

We ran cockroaches onto a perturbation device consisting of a rail-mounted cart that was accelerated horizontally by a manually keyed mechanism. In the reference frame of the cart, the cockroach center-of-mass received a large lateral impulse perpendicular to its heading. We recorded the trials using an overhead high-speed video camera and digitized the motions of the cockroach feet (tarsi). By applying methods developed in Revzen et al. [2008] and Revzen and Guckenheimer [2008] and used in Revzen [2009] Chapter 2, we used the tarsal trajectories in the body frame of reference to estimate the kinematic phase of the animals, and then fit a constant frequency model to the pre-perturbation phase data using linear regression. We used the residual phases derived from these regression models to test our neuromechanical hypotheses.

2.1 Lateral perturbation kinematics

2.1.1 Animals

We obtained the fifteen *B. discoidalis* cockroaches used in this study from a commercial supplier (Carolina Biological Supply Co., Gladstone, OR, USA) and kept them in large,

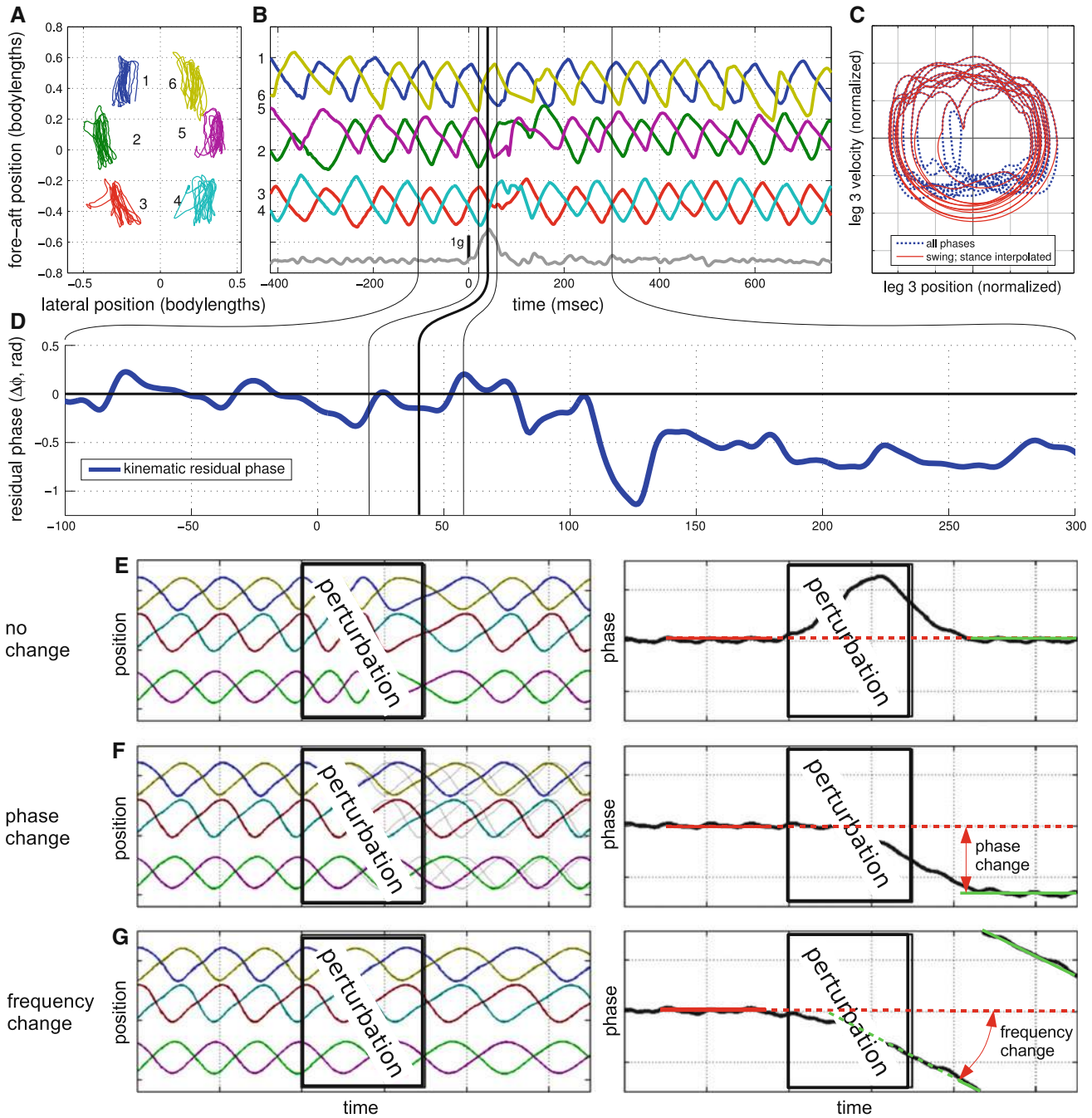

Fig. 2 From kinematics to kinematic phase. (**A**–**D** from typical animal trial) **A** Foot or tarsus trajectories over 1.1 s, in body coordinates, and fore-aft tarsus positions plotted over time (**B**). *Lower plot* in **B** indicates cart lateral acceleration (1 g scale bar shown at $t = 0$), with *vertical lines* indicating peak (*thick line*, 0.5 g *thin lines*) of perturbation which starts at $t = 0$. The complex-valued phase of the left hind leg (leg 3, *red* in **A**, **B**) is shown (**C**, *dashed blue*) together with the swing-only complex-valued phase, in which stances are linearly interpolated in complex argument and magnitude (**C**, *solid red*). The resulting residual phase for times–100 to 300 ms is shown in **D**, with corresponding times indicated by *vertical lines* in **B**. Theoretically plausible residual phase outcomes for perturbation experiments showing both (simulated) fore-aft leg positions over time on the *left* (**E**–**G**), next to the corresponding residual phase plot on the *right*. In **E**, we show an animal that slowed down during perturbation, but fully recovered to motions matching the motions extrapolated from pre-perturbation motion (*solid red* fitting region for regression model, *dashed red line* extrapolated model, *solid green* post-perturbation regression); this can be interpreted as the perturbation having broken the entrainment of body to system-level neural CPG, and that entrainment re-establishing itself post-perturbation. It is compatible with both Fig. 1A, B feedback alternatives. In **F**, we show an animal that recovers the same frequency at a phase offset; this can be interpreted as the re-entrainment locking on to a different stable relationship between the neural and mechanical oscillations, and is similarly compatible with Fig. 1A, B. In **G**, we show an animal whose frequency changes, as expressed by the non-zero slope of the residual phase trendline; such a change requires the system-level CPG to change frequency, and is therefore only compatible with the Fig. 1C feedback to the system-level CPG

open containers in a room with elevated moisture and temperature. They had access to dried dog food, fruit, vegetables, and water. We conducted trials at an ambient temperature of $27 \pm 2\,^{\circ}\mathrm{C}$ (mean, SD). Before each trial, we examined the cockroach for damage to its tarsi and carapace. Each animal was used in multiple trials. While downloading the videos between one trial and the next (typically 2 min in duration), we allowed the animals to rest by covering them with a dark cup.

2.1.2 Moving cart as a perturbation device

We induced lateral perturbations by having the animals run onto a cart that we then accelerated at a right angle to the direction of motion using a pre-loaded elastic pulley held fast by a magnetic lock (Fig. 3). When released, the cart translated with an acceleration of 1.5 ± 0.2 g over a duration of 100 ms and continued with a constant velocity until it hit breaking pads at the end of its track. The acceleration generated a specific impulse of $0.50 \pm 0.04\ \mathrm{ms}^{-1}$ in the lateral direction. Cart travel distance was nearly 1 m—sufficiently long so that in all analyzed trials the animal finished running the length of the cart before the final braking deceleration.

We marked the top of the cart with high-contrast circular markers (see Fig. 3D; circles of black paper with retroreflective stickers in their centers) at known locations encompassing the area occupied by the running animals and level with the surface on which they ran. We used these markers to track the cart, computing its acceleration using a Kalman smoother with a constant acceleration model (also known as a Rauch–Tung–Striebel smoother; Kalman 1960, Rauch et al. 1965; we used scalar covariance matrices, position 10^{-3} m, velocity $10^{-4}\ \mathrm{ms}^{-1}$, acceleration $10^{-5}\ \mathrm{ms}^{-2}$, observation noise 10^{-2} m). We also used the markers to compute a projective transformation that corrected for the changes in animal image due to changes in viewing angle and distance as the cart moved, giving what was effectively the view from a camera translating in parallel with the cart.

2.1.3 Protocol

We prodded the animals to run along the trackway shown in Fig. 3 and onto the cart. Careful adjustment ensured that the gap between the top of the cart and the trackway was only a few millimeters wide. We spanned this gap with a paper flap that was pushed aside when the cart moved, so the animals experienced neither any noticeable step nor break in the ground. We examined the animals' running for speed changes when crossing the trackway-cart gap, but found no significant differences. We found the same kinematic response at all positions along the cart, decreasing the plausibility that sensory information not associated with the perturbation affected the response patterns. In an additional set of control trials, speeds of blinded and/or antennal-ablated control animals (mean $\pm$ SD $= 33.5 \pm 7.6\ \mathrm{cm\,s}^{-1}$) showed no significant differences to intact animal running speeds ($36.2 \pm 7.0\ \mathrm{cm\,s}^{-1}$).

As soon as the animal was perceived to be on the cart, the operator released the cart by breaking the circuit powering the magnetic lock holding it in place. Taking into account human reaction times, animals were at least a body length from the cart edge by the time the cart began moving laterally. We ended trials when the cockroach touched any wall of the cart, or when the cart moved out of view. We rejected trials if the cockroach did not adopt a tripod gait for at least three strides prior to perturbation and three strides following perturbation, or if the cockroach antennae or feet came into contact with the side walls at any point during these requisite six strides.

2.1.4 Processing video data into residual phases

After we tracked the cart markers in each video frame, we projectively transformed the frames to a standard reference position, thereby canceling any warping and size changes due to changes in viewing angle. We then analyzed the corrected videos using a custom built video processing tool described more fully in (Revzen 2009) and briefly described below.

First, we auto-tracked the bodies of the animals by finding the axis of symmetry of their body silhouettes, thereby obtaining their position and orientation over time. We rotated the translated images to a registered position and orientation. We tracked the positions of the animals' tarsal claws (distal tips of the feet) on the registered videos using an additional custom tool. Both tools were written in MatLab version 6.5 (The MathWorks, Inc., Natick, MA, USA).

In our analysis, we used kinematic phases of individual legs, a global kinematic phase of the entire animal, and stance-leg-only and swing-leg-only global kinematic phase estimates (Revzen et al. 2008). We argue that the swing-leg-only global kinematic phase is the best proxy for the phase of a systems-level, reduced-order neural oscillator in the current experiment, as it combines all available sources of kinematic phase less affected by direct mechanical manipulation. The differences between swing-leg and stance-leg phase estimates reveals any biases that may be introduced to the global phase estimate by direct mechanical manipulation of the stance tarsi positions.

We constructed all phase estimates from motions of tarsi in the body frame of reference (Fig. 2A), taking only the fore-aft direction (Fig. 2B). To estimate instantaneous phase from a scalar-valued position time series with corresponding velocity, we first formed a complex-valued time series

$$z(t) = \overline{x}(t) + \mathrm{i}\overline{v}(t) \tag{1}$$

with real part equal to the studentized (i.e., mean subtracted and scaled to variance one) position and the imaginary part equal to the studentized velocity,

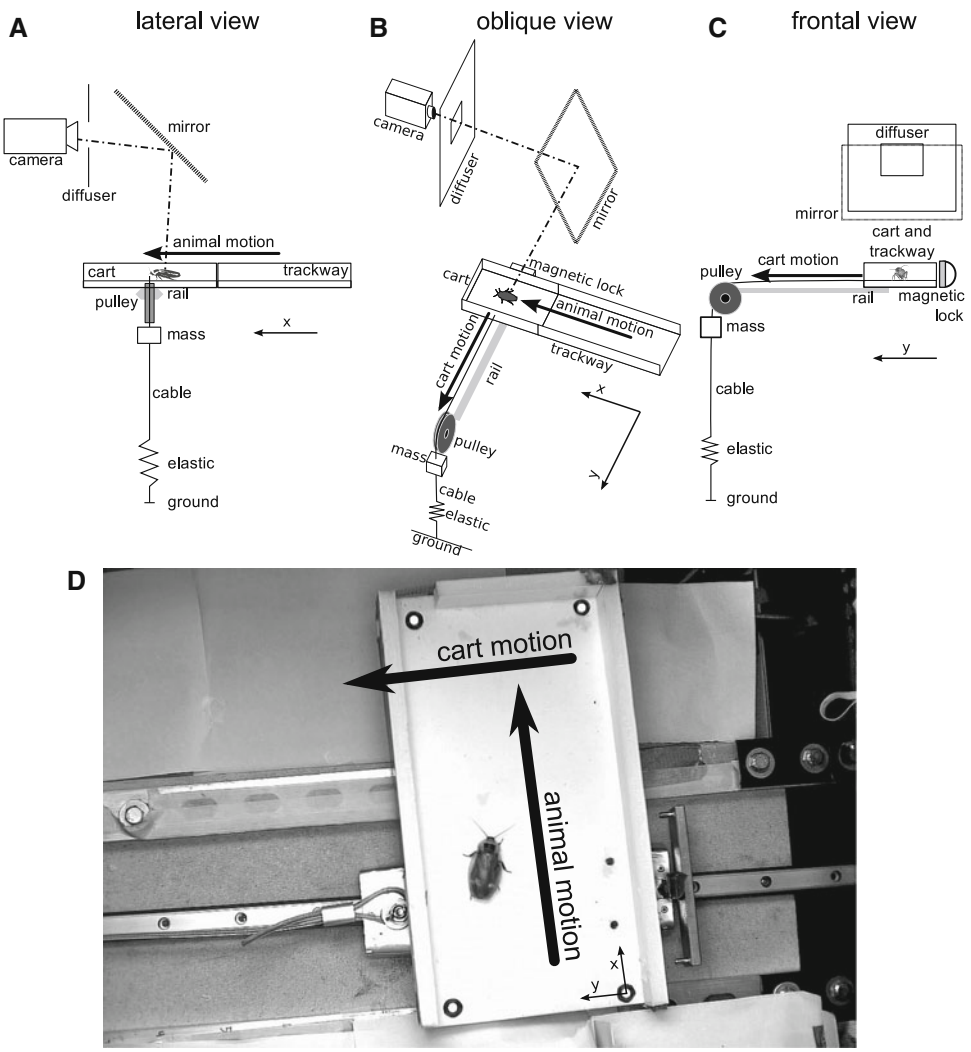

Fig. 3 Schematic of moving cart apparatus from lateral (**A**), oblique (**B**), and frontal (**C**) viewing directions (not drawn to scale). We placed the cart as the final section of a trackway (*white rectangles*). It ran on a rail orthogonal to the trackway direction (*light gray strip*). On one side, we held the cart fast with a magnetic lock (shown in **B**, **C** next to cart). On the other side of the cart, we tied it to a steel cable (*black line* running from cart to ground) that we ran through a pulley (*dark gray oval* in **B**, **C**), *rectangle* in **A**) and pulled taught using an adjustable elastic (collection of rubber bands, indicated schematically by zigzag on cable) and a mass (*white box* on cable below pulley). When the operator released the magnetic lock, the elastic accelerated the cart until it fully contracted to rest length. The cart continued to move at uniform speed, as we chose the mass to compensate for friction between rail and cart. The direction of motion of the animals was along the trackway (*thick arrow* labeled "animal motion" in **A**, **B**) and orthogonal to cart motion (*thick arrow* labeled "cart motion" in **B**, **C**). We filmed the motion with a high-speed video camera (camera seen in **A**, **B**; viewing animal along *dot-dashed lines*) that we mounted at a fixed position looking down on the trackway through a mirror (*rectangle with thick dashed lines*). We illuminated the trackway by bouncing a spotlight off a diffuser plate surrounding the camera lens (*thin-lined rectangle with rectangular hole* shown in all views), so that scene was illuminated from direction of camera, preventing shadows from appearing under the animal. **D** Photograph of an animal running on the moving cart. The cart had high-contrast markers near the corners on its surface. We constructed the cart from foam-core plates attached on top of a metal plate. The vertical metal plate on the left of the cart locked on to the magnetic lock, whereas the cart itself ran on a rail (metal strip running across the photograph and under the animal with dark top and bottom edges). A steel cable pulled the cart, providing the lateral accelerations. In the position shown, the cart has nearly moved an entire trackway-width to the left from its starting position. The edge of the trackway is visible at the *bottom right of the image*

$$\overline{x}(t) = \frac{x(t) - \langle x(t)\rangle}{\mathrm{std}[x(t)]}, \quad \overline{v}(t) = \frac{v(t) - \langle v(t)\rangle}{\mathrm{std}[v(t)]}. \tag{2}$$

Here, $\langle w(t)\rangle$ is the mean value, and $\mathrm{std}[w(t)]$ is the standard deviation of the random variable $w(t)$. For brevity, we refer to $z(t)$ as the "complex phase" time series (Fig. 2C). Velocity was computed using first-order finite differences of position. Since the complex phase series for the right-leading tripod (consisting of right-front, left-middle, and right-rear feet) fluctuated approximately one half-cycle out of phase with the series for the symmetric tripod, we multiplied them by -1 so that all complex phase series rotated around the

origin approximately in phase. We took the argument (polar angle) of the complex phase series as our instantaneous phase estimates for individual legs,[1]

$$\phi(t) = \arg(z(t)). \tag{3}$$

To construct a continuous phase variable from discrete temporal events that occur at known phase increments (e.g., posterior extreme position (PEP) events), we linearly interpolated phase in time.

We manually identified the start and end of the perturbation from the cart acceleration. Using a window starting 150 ms ($t_{1\mathrm{pre}}$) and ending 40 ms ($t_{2\mathrm{pre}}$) prior to onset of perturbation, we fit a linear (constant frequency) model to phase. We subtracted this model from each trial's phase then offset these data so as to have zero mean during the fitting window to obtain residual phase (Fig. 2D),

$$\begin{aligned}\Delta\phi(t) = \phi(t) &- \left\langle \phi(t) \middle| t \in [-t_{1\mathrm{pre}}, -t_{2\mathrm{pre}}] \right\rangle \\ &- \left\langle \dot{\phi}(t) \middle| t \in [-t_{1\mathrm{pre}}, -t_{2\mathrm{pre}}] \right\rangle \left(t - \frac{t_{1\mathrm{pre}} + t_{2\mathrm{pre}}}{2} \right),\end{aligned} \tag{4}$$

where $\langle w(t) | t \in [a, b] \rangle$ is the mean value of $w(t)$ over the time interval $[a, b]$. We used this residual kinematic phase to test for changes in the animals' rhythm, as follows. When the residual phase was a horizontal line (slope of zero) with an intercept of zero (Fig. 2E), it represented animals that continued running at the same frequency and phase as they did prior to perturbation. A horizontal line with non-zero intercept (Fig. 2F) implied a phase change, and any non-zero slope (Fig. 2G) represented a frequency change.

2.1.5 Kinematic outcome classes

The kinematic state of an animal following a periodic gait is fully represented by its kinematic phase. This implies that whenever some outcome is hypothesized to depend on posture at perturbation, one may operationalize this hypothesis as a statistical test for phase at perturbation ϕ_0 being a statistically significant predictor of the outcome.

In our experiment, we partitioned kinematic responses to lateral perturbation into two classes—C_0 and C_1—based on ϕ_0 values predicting two different velocity profiles during recovery. Animals perturbed in one half-cycle of the stride responded differently from animals perturbed in the other half-cycle. It is reasonable, from a physical standpoint, for multiple responses to occur because an animal with two legs of a tripod in contact with the substratum on one side may not respond to a lateral impulse in the same manner asan animal with only its middle leg in contact with the substratum on that same side.

2.1.6 Improving the phase estimates

Since the perturbation we consider here directly manipulated the foot positions in the animal body reference frame, we suspected that data from the stance feet would give a phase estimate that is inconsistent with the system-level phase of the animal. To determine whether this effect appeared in our data, we compared the residual from our global kinematic phase to that of "swing-only" and "stance-only" phases. To estimate swing-only phase, we computed complex phase time series for each individual tarsus, then for each stance period, we linearly interpolated the argument and amplitude of the complex phase from its touchdown value to its lift-off value, which is equivalent to imposing a constant frequency model (Fig. 2C, dashed is leg 3 complex phase for all times; solid is with stances interpolated). We then took the argument of the mean of the six corrected complex phase time series as the global instantaneous swing-only phase. We computed global instantaneous stance-only phase similarly, except that complex phase was interpolated during swing instead of stance. Noticeable differences between stance-only and swing-only residual phase estimates appeared 50 ms after onset of perturbation and lasted for almost a step. During this time, the average stance residual showed a small increase or decrease depending on which tripod was in stance during the onset of perturbation (differences between C_0 and C_1 class means). This effect was also evident in the global phase, but not in the residual obtained from swing data. Since the unloaded swing feet should better reflect any change in timing of motor commands to the legs within 16 ms (Dudek and Full 2007), the most parsimonious explanation is that this effect arose from a mechanical perturbation. Consequently, we take the swing-only residual as the most representative kinematic estimate of the system-level state of the animal under these perturbation conditions. In the sequel, use of the term "(kinematic) phase" refers to swing-only phase, unless otherwise specified.

2.1.7 A statistical test for significance of velocity outcome classes

There is no obvious choice of a parametric test for the statistical significance of the ability of an angle variable—the predictor phase ϕ_0 taken before onset of perturbation—to predict the difference between two classes of real time series—the velocity of the animals over time. We therefore used a bootstrap analysis and validated our inference using surrogate data (Politis 1995, 1998).

We computed a predictor phase ϕ_0 by taking the circular mean (Fisher 1993) of a phase time series in a half-step-long

[1] When the series all have the same amplitude this is precisely the circular average (Fisher 1993) of their phase angles.

(22 ms; 1/2 t_{step}) window ending at onset of perturbation (t_{on}),

$$\phi_0 = \arg\left(\left\langle \exp(\mathrm{i}\phi(t)) \,|\, t \in [t_{\text{on}} - \frac{1}{2}t_{\text{step}}, t_{\text{on}}]\right\rangle\right), \tag{5}$$

where $\exp(\mathrm{i}\phi)$ is the complex exponential of the imaginary quantity $\mathrm{i}\phi$. Our prediction classified trials into one of two classes C_0 and C_1 based on the sign of $\sin(\phi_0 - \Phi)$ for some optimally selected choice of Φ, thereby partitioning the circle of possible phase values into halves with the transition between classes occurring at phases Φ and $\Phi + \pi$.

We assessed the quality of a classification of trials into C_0 and C_1 using the root mean squared (or L2 norm) difference between the class means of the forward velocity time series (Vx) in a time interval starting 50 ms ($t_{1\text{post}}$) and ending 150 ms ($t_{2\text{post}}$) after onset of perturbation. That is, with Vx_0 and denoting Vx_1 the mean forward velocity of C_0 and C_1, the quality of classification is given by

$$\| Vx_0 - Vx_1 \| = \left(\int_{t_{1\text{post}}}^{t_{2\text{post}}} |Vx_0(t) - Vx_1(t)|^2 \, \mathrm{d}t \right)^{1/2}. \tag{6}$$

This provided a statistic measuring class separation and thus prediction quality using a kinematic variable that was not directly manipulated by the perturbation because it is derived from velocities in a direction orthogonal to the perturbation. Our algorithm selected the Φ producing the best classification with respect to this quality measure. We then tested this classification for statistical significance using all available kinematic data.

We formulated a test of statistical significance by comparing the classification quality measure of the real data with the classification quality measure of surrogate (randomized) data for which the relationship between the predictor ϕ_0 and the outcome (velocity time series) was rendered insignificant by adding a uniformly distributed random phase to ϕ_0. We calculated the fraction of surrogate datasets that produced a classification of comparable quality to that of the animal data; this fraction is the probability of a false positive under the null hypothesis of no predictive ability. The approach is also known as using "percentile confidence intervals generated from a bootstrap" (Politis 1995, 1998).

We examined the distribution of classification quality obtainable by choosing Φ where this selection was applied to ensembles of trials generated from the following processes:

H_1 animal data: comprising N^2 bootstrap samples of the actual experimental trials.

$H_{0(a)}$ simple surrogates: comprising N^2 bootstrap samples with an added (uniformly distributed) random offset to the phases in each trial. This randomizes ϕ_0 in each sample, while maintaining all internal correlations within each trial.

$H_{0(b)}$ bootstrapped surrogates: comprising N randomized trials as per $H_{0(a)}$. Instead of using each bootstrap collection of trials once, taking the best classification quality for N bootstraps of the surrogate data. This controls for bias introduced by picking the best classification, as differences between $H_{0(a)}$ and $H_{0(b)}$ distributions reflect this selection bias.

When the classification quality generated by the H_1 process fell well outside the distributions generated in the two H_0 processes, we concluded that the choice of Φ did partition the trials using their predictor phases ϕ_0 into statistically significant classes C_0 and C_1 of velocity outcome.

2.1.8 *Controlling for individual variation in the predictor phases*

One potential cause for the appearance of classes in the residual phase time series could be individual variation in predictor phases. We tested the hypothesis that the classes C_0 and C_1 were an outcome of inter-individual variation where some individuals could be biased toward being in C_0 and other individuals biased toward being in C_1.

If an individual falls preferentially in any one class, this implies that the ϕ_0 values for this individual's trials are biased toward appearing in this class. We developed a test for comparing the hypotheses: $H_{0(\phi)}$—the ϕ_0 angles of individual animals are drawn from uniform distributions; $H_{1(\phi)}$—each animal has a (possibly different) preferred phase angle θ such that ϕ_0 values for trials of this animal are more likely to be close to θ than far from θ.

The uniform distribution on angles has the property that if angles θ_i are uniformly distributed, their differences are also uniformly distributed (This is not true of uniform distributions on a real interval. The property for uniform circular distributions follows from the rotational invariance of the distribution implying rotational invariance of the differences). However, if there is any sort of preferred angle θ for each individual the differences are more likely to be closer to zero than to other angles. We combined the differences of ϕ_0 values of random pairings of same-individual trials in a single pool and used the Rayleigh Test (Fisher 1993) for circular uniformity—effectively testing $H_{0(\phi)}$ against an $H_{1(\phi)}$ consisting of a unimodal Von-Mises distribution for the phase differences.

2.2 MAP measurements

To examine whether the activation of key leg control muscles follow predictions from instantaneous kinematic phase, we measured the MAPs from muscles 178 and 179 (Carbonell 1947) in the metathoracic leg before, during and after the lateral cart perturbation. This muscle is a coxa-femur extensor recruited during running and shares the same excitatory (D_f)

motor neuron as muscle 178, located dorsally. Because this muscle is innervated by a single motor neuron that generates stereotyped bursts of MAPs during free running, understanding its contribution to generating rhythmic movement is greatly simplified.

2.2.1 Animals

Animals used for this experiment were obtained and raised under similar conditions to those used in the kinematic experiments. To prepare specimens, we followed commonly used EMG procedures for cockroaches (see Ahn and Full 2002; Sponberg and Full 2008; Watson and Ritzmann 1998a, b). First, we cold-anesthetized animals for 30 min or until movement stopped. We removed both pairs of dorsal wings using dissection scissors. We then mounted animals ventral side up to expose the coxa and made two small holes in the cuticle with size 0 insect pins along the axis of the muscle. After stripping the insulation of 50 μm silver wires (California Fine Wire Company, Grover Beach, CA, USA) and creating small balls at the end of the wires with heat, we carefully inserted the tips under the exoskeleton. These wires were used for bipolar recordings of muscle action potentials. We covered the area with a few drops of cyanoacrylate, being careful to avoid the joints. We placed a third wire on the dorsal side of the first abdominal segment to serve as a reference electrode. Finally, the three wires were braided together to form a tether and glued onto the pronotum. We then placed the animals in a dish and gave them at least 1.5 h to recover at room temperature (25 °C).

2.2.2 Protocol

We connected the electrodes to an AC amplifier (Model P511, Grass Technologies, West Warkwick, RI, USA) that amplified the signal 5,000-fold. To monitor the acceleration of the cart, we used a three-axis MEMs accelerometer (MMA7260, Freescale Semiconductor, Austin, TX, USA) with a dynamic range of ±2 g mounted directly onto the metal base of the cart. The accelerometer was calibrated using a two-point calibration method (Spence et al. 2010). We acquired data on all channels at 10 KHz. During the experiments, we kept the room temperature between 27 and 30 °C. We elicited an escape response in cockroaches by probing the posterior abdominal segment and cerci. The animals ran onto the cart, at which point we triggered its release. We used the same trial acceptance criteria as the kinematic phase experiments (Sect. 2.1.3).

EMG recordings and accelerometer signals were synchronized with the video data using an external trigger switch. All data processing was performed using custom MatLab scripts (MathWorks, Natick, MA, USA). For analyzing EMG signals and determining spike times, we digitally filtered the signals using a band-pass filter between 100 and 1,500 Hz and a notch filter at 60 Hz. Spike times were determined by computing local minima of spikes identified at a fixed threshold. We filtered the accelerometer data using a low-pass second-order Butterworth filter with cut-off frequency of 30 Hz.

2.2.3 Data processing

We performed statistical hypothesis testing on the EMG data using Minitab (Minitab, State College, PA, USA) to test for the effect of our perturbation on the clock-like signal from muscles 178 and 179. For multiple regression analysis in the presence of co-variates, we used an ANCOVA for continuous variables (inter-burst and inter-spike intervals) and a Cochran–Mantel–Haenszel (CMH) test for categorical variable (number of spikes per burst).

To compute the residual phase of the MAP data, we computed the average inter-burst interval (IBI) prior to perturbation to create a constant frequency linear oscillator model and subtracted this model from each trial's measured burst times. We represent the notion of phase as a fraction of the time between burst events by linearly interpolating the phase between the residual phase values.

3 Results

3.1 Collective kinematic outcomes

We used a total of 15 animals and 41 trials. The animals ran at 0.26 ± 0.03 ms^{-1} (mean, SD, across trials) at a frequency of 11.0 ± 0.2 Hz. Lateral perturbation velocities 0.50 ± 0.04 ms^{-1} were typically of a magnitude double that of the forward velocity.

The overall outcomes of lateral perturbation are shown in Fig. 4 with 1 and 99 % confidence intervals obtained from a bootstrap. Frequency decreased by 0.6 Hz as expressed by the negative slope of the Fig. 4A. Forward velocity (Vx) decreased from 26.1 ± 0.3 to 20.2 ± 0.8 cm s^{-1} found in the mean shift of Fig. 4C. Lateral velocity (Vy) decreased to -34.5 ± 0.9 cm s^{-1} followed by a return to zero and overshoot to 17.0 ± 0.3 cm s^{-1} before returning to zero (Fig. 4D). Ground speed showed a transient increase to 45.5 ± 0.9 cm s^{-1} from the initial speed of 27.3 ± 0.4 cm s^{-1} (Fig. 4E). Yaw, the direction of the body axis with respect to the cart, changed at its peak by $28.6° \pm 0.7°$ (Fig. 4F).

Changes appeared at a delay from onset of perturbation. The earliest change manifests in lateral velocity (Fig. 4D) which became significant within less than 25 ms. This was followed by ground speed and yaw angle at 40 ms (Fig. 4E, F). Forward velocity showed a change in trend at 70 ms. By 250 ms, mean yaw angle was between −5° and 10°, and by 300 ms the confidence interval for lateral velocities included zero.

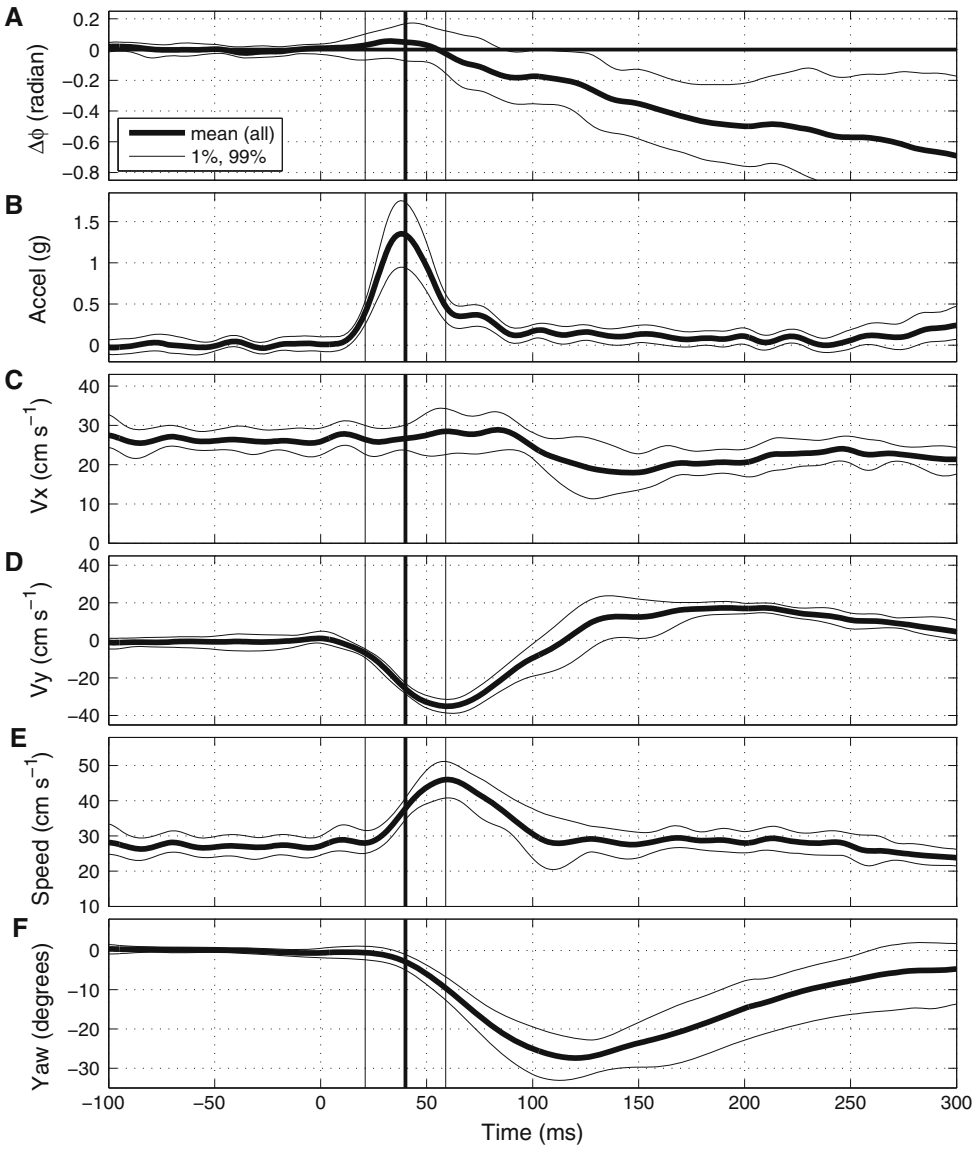

Fig. 4 Response of residual phase and center of mass kinematics to a lateral perturbation as a function of time. **A** Residual phases obtained by subtracting from the phase estimate a linear regression model fitted to the phase at times −0.100 to 0 s as in (4). Time 0 indicates onset of perturbation, *vertical thick black line* indicates peak acceleration, as can be seen from the cart acceleration plot (**B**; *thick line* is mean; *thin dashed lines* represent 1 and 99 % confidence intervals of bootstrap mean). **C** Animal velocity in direction of trackway axis, Vx; **D** lateral velocity across trackway, Vy; **E** total speed of the animal; and **F** yaw angle of body axis relative to the trackway axis

3.2 Phase predicted two classes of outcomes

We found that the population of trials can be partitioned into two classes of outcomes based on the animals' phase at onset of perturbation ϕ_0. We partitioned the circle of possible phase values ϕ_0 into two halves, choosing the partition that induced the maximal separation between forward velocity (Vx) time-courses of the two classes. We computed ϕ_0 as the (circular) average of the phases in a 0.022 s (half-step long) window ending at onset time of perturbation. Since the choice of which phase to label 0 is arbitrary, we chose our phase of 0 so that the trials with $0 < \phi_0 < \pi$ form class C_0, and the trials with—$\pi < \phi_0 < 0$ form class C_1 (red and blue colors in Fig. 5). At peak perturbation, animals in class C_1 were in a stance of what we designated as a "left tripod" (left front, right middle, left hind), whereas animals in class C_0 were in a stance of a "right tripod" (right front, left middle, right hind).

We tested the statistical significance of the classification based on ϕ_0 values by examining the bootstrap distribution of class lateral velocity separation and comparing this to distributions generated from randomized (surrogate) null models. We estimated the quality distributions by executing 2,500 bootstrap replications each of surrogate and unmodified data. The distributions of the results are in Fig. 6. The P values, we found were 0.023 for simple surrogates $H_{0(a)}$ and 0.028 for bootstrapped surrogates $H_{0(b)}$, rejecting both null hypotheses. These results showed that the separation computed for our dataset was typical of the bootstraps of the data (i.e., it is a robust outcome), and atypical ($P < 0.05$) of both $H_{0(a)}$ and $H_{0(b)}$ null hypotheses. For data that do not truly comprise two classes (such as our surrogates), selecting the partition of ϕ_0

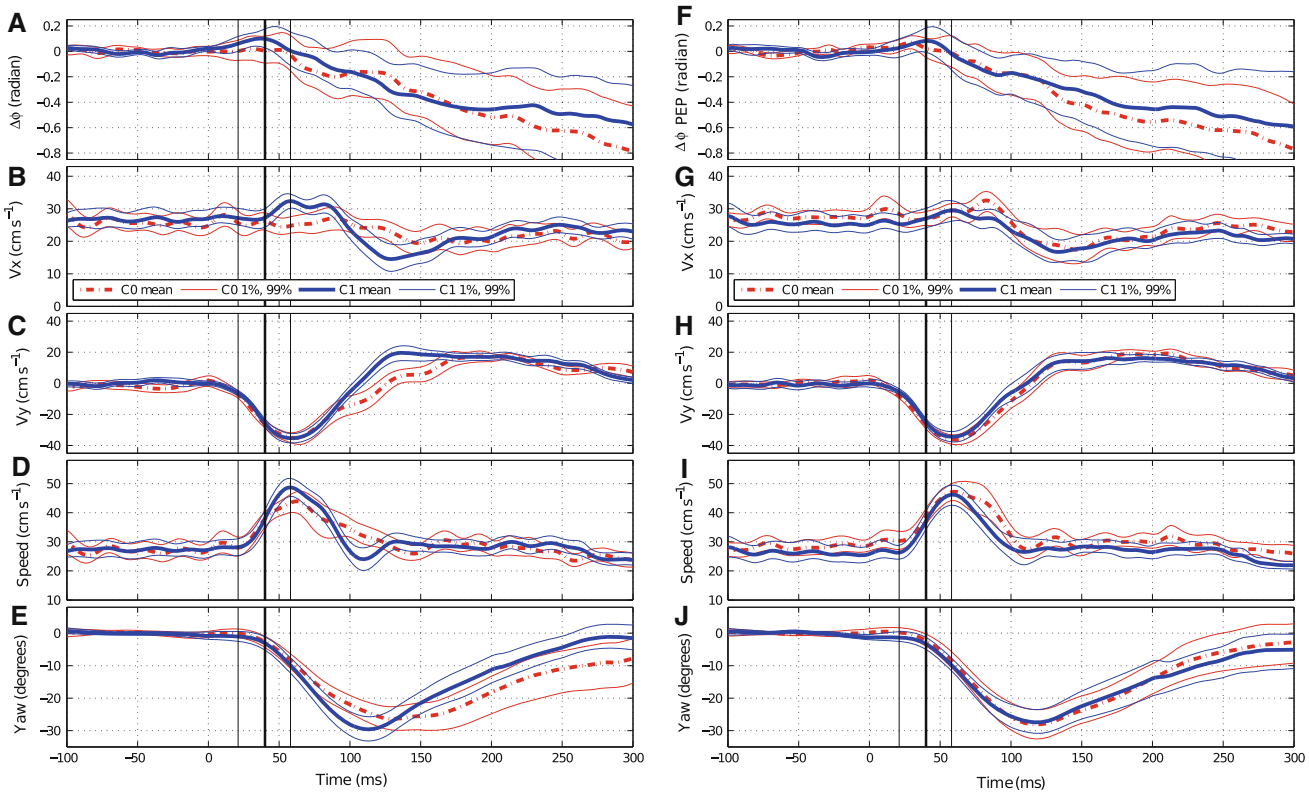

Fig. 5 Outcomes of lateral perturbation as a function of time and class. Trials were grouped into two classes (C_0 "right tripod" and C_1 "left tripod"). Time 0 indicates onset of perturbation, *vertical thick black line* indicates peak cart acceleration. **A** Residual phases; **B** animal velocity in direction of trackway axis, Vx; **C** animal lateral velocity across trackway, Vy; **D** total speed of the animal; **E** yaw angle of animal body axis relative to the trackway axis. Trials were classified into C_0 or C_1 based on their phase in the window spanning −0.022 to 0s (half-step prior to onset of perturbation). Trials fell into two classes of outcome: C_0 (*thick dense dashed red line* showing mean; *thin red line* showing 1 and 99 % of the bootstrap means) and C_1 (*thick blue line* show showing mean; *dashed thin blue line* showing 1 and 99 % of the bootstrap means). C_0 had a "right tripod" in stance where the right front, left middle, right hind legs were in stance phase during perturbation. C_1 had a "left tripod" where the left front, right middle, left hind legs were in stance phase during perturbation. **F**–**J** Same as **A**–**E**, but with classification computed using phase estimate derived from discrete events using the PEP of the legs as done routinely. Differences between classes that appeared clearly with the instantaneous kinematic phase computation used in **A**–**E** are not observed. This likely results from the larger uncertainty about phase that prevents the separation of a large fraction of trials

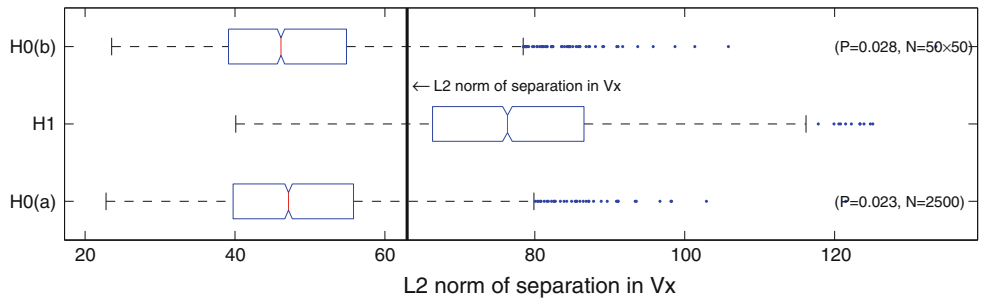

Fig. 6 Bootstrap test results for significance of outcome classification. Each of the three Tukey *box-plots* showed a distribution containing 2,500 bootstrap replicates. The H_1 plot represents a distribution created by simple bootstrapping—trials re-sampled with replacement. $H_{0(a)}$ is similar, except that we added (independently and identically distributed uniform) random phase offsets to each trial in each replication creating surrogate data. $H_{0(b)}$ consisted of 50 bootstraps, each of which we randomized in phase similarly to $H_{0(a)}$ and then bootstrapped to create 50 samples from each randomization instead of just one as in $H_{0(a)}$. Each Tukey *box-plot* shows a box for the inter-quartile range, with a narrow neck indicating the 95 % confidence interval of the median. Wicks go out to the first data point outside the 10th and 90th percentiles, with points outside that range marked as *dots*. The ordinate of the plot is the RMS difference between class means of Vy (Fig. 5D shows actual classes; value indicated here by *thick black line*). We used the bootstrap distributions to estimate *P* values with respect to the null (values on right edge of plot). The experimental value is closer to the mode of the null hypotheses than the mean bootstrap value of H_1, therefore our *P* values are conservative. Results showed that classes C_0 and C_1 were a statistically significant feature of the data

values that induces the greatest class separation is more than 95 % likely to induce less separation than we observed in our data and in a large majority of randomly selected resamples from our data. This indicates that the classification we extracted is a reliable feature of the data rather than an artifact of data analysis. We performed this same analysis using the phase estimate derived from the PEPs of the legs (Fig. 5F–J). In this case, the distribution obtained for class forward velocity separation (Fig. 5G) under the H_1 hypothesis was statistically indistinguishable from the surrogates $H_{0(a)}$ and $H_{0(b)}$ ($P > 0.1$ in both cases). We attribute this loss of significance to the lower temporal resolution afforded by a phase estimate derived from discrete events (i.e., a non-instantaneous phase estimate).

The classes C_0 and C_1 were divided with 25 trials in C_0 and to 16 trials in C_1, giving a $\chi^2 = 1.98$ with $P = 0.16$. The trials thus fell into classes with probabilities indistinguishable from random. The Rayleigh test applied to bootstrap samples of the 32 trials which came from animals that ran more than one trial gave Rayleigh test statistics with 10 and 90 % quantiles of 0.09 and 1.87, respectively, and a mean of 0.8, corresponding to P values all of which are larger than 0.1, and thus robustly (for nearly all bootstraps) failed to reject the null hypothesis of uniformly distributed ϕ_0 values per individual. We conclude that our classification was not produced by individual variation in animal responses, or in other words that no individual experienced the perturbation in any class (i.e., "left tripod" or "right tripod") more often than expected at random.

3.3 Kinematic differences between the classes

Comparing the results in Figs. 4 and 5, the structure generating outcome variability in Fig. 4 becomes evident. Whereas Fig. 4C–F showed changes in variability around the mean at different delays from onset of perturbation, the corresponding plots in Fig. 5B–E showed that each class has uniform within-class variability over time. Thus, the large changes in variability in Fig. 4 are accounted for by distributing outcomes into two classes. Furthermore, Fig. 5F–J contains the kinematic outcomes arising from the classification obtained from the PEP phase estimate. The lack of statistical significance for this classification is manifest in the indistinguishable kinematic outcomes of the two classes.

The C_1 trials (left tripod down) showed initial statistically significant, but small in magnitude increases in phase and forward speed from zero at approximately 0.045 s after onset of perturbation (Fig. 5A, B; solid blue) relative to C_0 trials. We suspected that this change might not be due to neural clock changes and is instead due to direct mechanical effects of body yaw on the stance legs. As our phase estimate uses the swing tarsi in the body frame of reference, it is partially isolated from mechanical influence on the stance tarsi. However, at the moment of lift-off, because stance tarsi are attached to the ground, yaw might induce a systematic structure in the velocities of tarsi which carries through into swing and could appear as a change in phase. To inform our understanding of how much of the C_1 class-specific phase increase is due to this effect, we introduced a simulated pattern of unperturbed tarsus positions into a body frame of reference derived from experimental data, then clamped the stance legs to the world frame at touchdown, and relaxed them back to their unperturbed body frame position within 16 ms—the rate of mechanical relaxation identified by Dudek and Full [2007]. The goal of this simulation of "feed-forward" tarsus motions attached to experimentally derived center of mass (COM) trajectories is to reproduce a plausible model for the motions of the tarsi of an animal which is activating its legs without any feedback modulation. These simulated animals exhibited a class-specific phase change similar to that seen in the experimental data in the 0.045s region under discussion. If that phase change is taken into account, the confidence intervals for C_1 in Fig. 5A would include zero. We conclude that the small increase we observed is likely due to this mechanism.

C_1 trials lateral velocity recovered and overshot faster (Fig. 5C, solid blue). They reached the peak overshoot value 0.050 s before C_0 trials (Fig. 5A, B, dashed red). Yaw of C_1trials fully recovered within less than 0.30 s (Fig. 5E, solid blue), whereas animals represented in C_0 trials (Fig. 5E, dashed red) never recovered their original yaw angle within the period measured.

3.4 Residual phase change represents a frequency change

Starting with onset of perturbation (time = 0), animals showed no significant change in kinematic phase for 0.030 s—nearly the duration of an entire step. After that time, frequency increased (see Fig. 4A mean), but this increase was statistically significant for less that 0.025 s in the first half of the perturbation, and only in the C_1 class of trials (Fig. 5A, solid blue). Within the next 0.050 s, residual phase changed to follow a new trend-line, corresponding to a >5 % decrease in the frequency of animal tarsus cycling, decreasing from 11.0 ± 0.2 Hz by 0.6 Hz.

We conclude that kinematic evidence for neural feedback, in the form of a persistent frequency change, appeared in the recovery of cockroaches from lateral perturbation. Frequency decrease appeared at a delay, and the delay was not a function of the animal's posture (i.e., C_0 vs. C_1), although the actual change in kinematics —differences in COM velocity—was posture (class) dependent.

3.5 Muscle action potentials

We collected 37 trials from 7 male cockroaches with a mass 2.32 ± 0.32 g. Animals ran at a speed of 0.362 ± 0.070

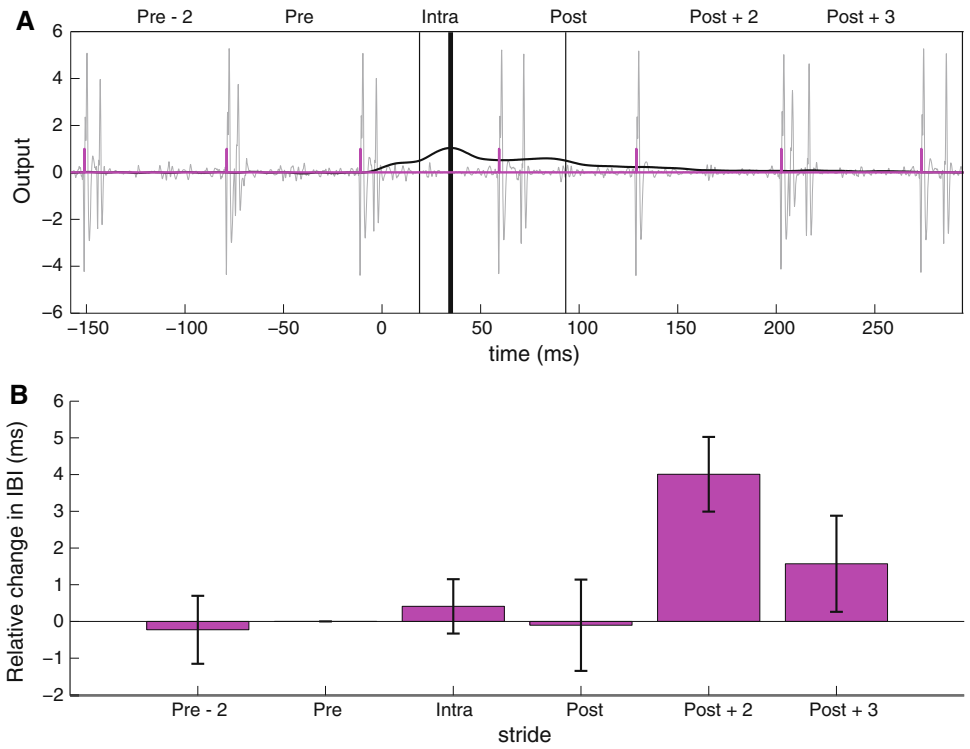

Fig. 7 Muscle action potential phase response to lateral perturbation. **A** Muscle action potentials from muscle 178 and 179 for single, representative trial. MAPs are shown in *gray*. The *magenta* spikes represent the onset of the burst. One burst occurred per stride. *Black curve* shows cart acceleration. Intervals represent two strides before the perturbation (Pre-2), one stride before (Pre), during (Intra), one stride after (Post), two strides after (Post-2) and 3 strides after the perturbation (Post-3). **B** Mean relative change in MAP IBI as a function of perturbation state. IBI increased two and three strides after the perturbation representing a decrease in stride frequency. *Bar* represent ±1 SE

ms^{-1}. MAP recording allowed easy discrimination of spikes (Fig. 7A) as in Sponberg and Full [2008]. MAP IBIs during and one stride after the perturbation showed no significant change compared to pre-perturbation intervals (Fig. 7B). Two strides after the perturbation (Post + 2; Fig. 7B), we found a significant median period change in IBIs relative to the pre-perturbation strides of 4.9 ms (t test for relative mean, $P \leq 0.001$). Results suggest neural feedback to control muscles 178 and 179 occurs approximately 100 ms after perturbation. The increased IBI duration remained three strides after the perturbation (Post + 3; Fig. 7B) indicating a persistent decrease in frequency. Analysis of inter-spike intervals (ISI) revealed no changes when comparing pre- and post-perturbation strides (t test, $P = 0.16$). Since speed and ISI were correlated, we tested for the effect of speed (F test regression DF = 1,361, $P \leq 0.001$) and found no statistically significant difference (F test DF $= 1, 361$, $P = 0.29$). A non-parametric test to control for non-normal distributions did not change the statistical outcome (Kruskal Wallis test, $P = 0.23$). Likewise, we found no statistically significant changes in the number of spikes per burst when comparing the number of spikes pre- and post-perturbation (Pearson χ^2 test, $P = 0.74$) even after correcting for the possible effect of individuals (CMH test, $P = 0.32$). Thus, neither ISI nor the number of spikes per burst changed when comparing pre- and post-perturbations strides suggesting that a change in frequency of the clock-like signal to this putative control muscle is the dominant source of neural feedback.

We subjected the linearly interpolated MAP residual phase time series to the same bootstrap analysis method used to derive confidence intervals for the kinematic phases. Post-perturbation changes in MAPs were consistent with the predictions made by measurements of instantaneous leg kinematic phase and frequency (Figs. 4A, 10). Specifically, the decrease in frequency as measured by the increase in IBIs and the qualitative structures of the interpolated MAP residual phase estimate compared to the kinematic phase estimate with overlapping 98 % confidence intervals are consistent with neural feedback occurring near 100 ms corresponding to one or more strides after perturbation.

4 Discussion

4.1 Kinematic phase reflects neural feedback to a system-level oscillator

Instantaneous estimates of kinematic phase and frequency can serve an important tool to propose neuromechanical control hypotheses that would otherwise have been difficult to identify. By using more readily collectable motion data, the response to complex perturbations can be compared quantitatively to that behavior projected into the future without perturbation. The high temporal resolution can lead to the discovery of new kinematic patterns not observed by traditional approaches. Kinematic phase analysis can lead to tests

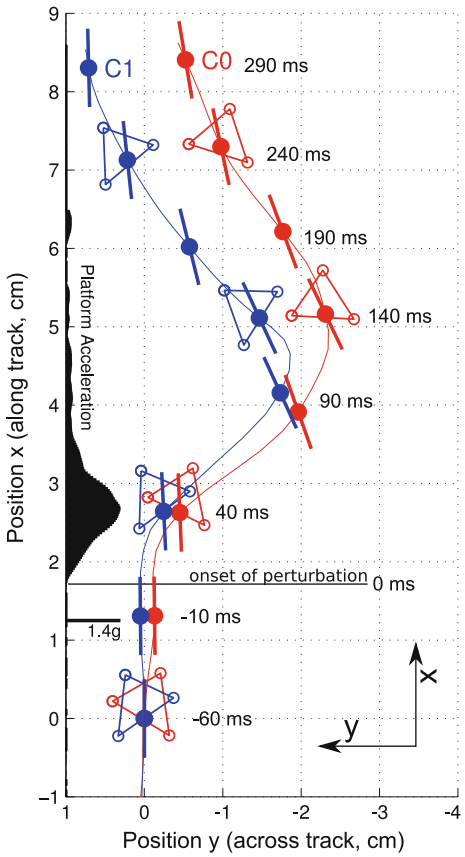

Fig. 8 Summary of experimental results showing the mechanical differences between classes C_0 and C_1. Average animal positions for each class are shown from a top view (*X* and *Y* indicated to match Fig. 3) with a series of symbols plotted at positions sampled from the data at 50 ms intervals. Stance tarsus positions indicated by *empty circles*, animal COM trajectories are traced with a *solid line*, COM indicated by a *large dot*, and body axis orientation indicated by a *line passing through the COM symbol*. Cart impulse is shown in *black*. Animals in C_0 trials (*right*; *red*) experienced the brunt of the perturbation while in stance on the right tripod (i.e., front right, middle left and hind right). As the cart accelerated to the left, the animals' inertia pulled their bodies to the right. In this posture only one tarsus had claws that can engage to exert a counter-force (*circles around middle leg foot*). In contrast to C_0, in C_1 trials (*left*; *blue*; *left tripod*—front left, middle right and hind left) animals had two tarsi whose claws can engage, providing more corrective force, and the ability to correct torque independently from force by trading off front and hind leg lateral forces. The larger mechanical disturbance experienced by C_0 manifests as an increase (at 90 ms snapshot) followed by a decrease (at 190 ms snapshot) in COM speed (a complete comparison of COM speed by class in Fig. 5D)

of reduced-order, system-level hypotheses not possible with reductionist approaches focusing on the details of a single subsystem.

Here, we used lateral perturbation in cockroaches to highlight the utility of using kinematic phase to examine the relationship of multiple oscillating units, be they found in neurons, muscles, appendages or whole bodies. Using instantaneous kinematic phase on a complex perturbation with six rhythmically oscillating legs, we discovered neural feedback to the system-level neural oscillator or CPG (Fig. 1C). We resolved this feedback to the duration of a single step or stride (Fig. 4A). Our results are consistent with the first efforts (Grillner 1972; Wilson 1961) to demonstrate sensory feedback to the CPG period. However, here we focus on a system with many oscillating subsystems and their coupling to the mechanical system in a freely moving animal and not on the response of a specific sensor or local feedback pathway. Our kinematic phase approach permits quantitative exploration of what Marder et al. [2005] describe as "a network of multiple higher order neurons" and Büschges et al. [2011] refer to as "descending inputs from higher centers which initiate CPG activity, regulate CPG frequency, and alter CPG output to maintain whole body equilibrium (posture) and produce appropriate goal-directed behaviour."

Our kinematic phase results reflected proposed control architectures that couple feed-forward and feedback systems comprised of both neural and mechanical elements (Fig. 1). The lack of change in kinematic phase early in recovery (Fig. 4A) can be most parsimoniously explained by mechanical self-stabilization (Fig. 1A). Between two to three steps later, a significant change in kinematic phase of the mechanically unconstrained swing legs indicates the appearance of neural feedback to the system-level CPG (Fig. 1C). For the first 50 ms from onset of lateral perturbation to well beyond the peak of perturbation, running cockroaches followed the pre-perturbation feed-forward motion model. Neither the residual phase (thick dark line, Fig. 4A) nor velocity and yaw (thick dark lines, Fig. 4C–F) were changed relative to their pre-perturbation ranges. The most likely interpretation of these results is a reliance on mechanical feedback (Fig. 1A). Schmitt and Holmes (2000a, b) found that a horizontal plane mass-spring model (Lateral Leg Spring, LLS) that moves forward by bouncing side-to-side can self-stabilize to lateral perturbations with little or no neural feedback and recover rapidly in body orientation and rotational velocity (Schmitt et al. 2002). Experimental perturbations fit these mechanical self-stabilizing models with additional assumptions of specific feedback pathways (Jindrich and Full 2002). More anchored hexapedal models with various forms of simulated proprioceptive feedback and heading control (Kukillaya and Holmes 2007, 2009; Kukillaya et al. 2009) affirm that feed-forward neural activation patterns can provide recovery from lateral impulses such as the perturbation we applied here.

Kinematic phase data alone are insufficient to reject tracking feedback (Fig. 1B) when no change in residual phase is observed. Direct measurement of sensory or motor pathways are required. Sponberg and Full [2008] showed no change in the MAPs feed-forward pattern for the same control muscle measured here, when cockroaches ran over flat versus rough terrain with obstacles three times their hip height. In this study, we discovered that the same leg control muscle

did not alter its feed-forward IBI until 100 ms after peak perturbation and 140 ms after perturbation onset that corresponds to one or more strides after the maximum perturbation (Fig. 7). Yet, our kinematic data show a nearly-complete recovery of lateral velocity (Fig. 4D) before the MAP interburst duration change (Fig. 7B) or the residual kinematic phase changes (Fig. 4A). Certainly, one cannot rule out the possibility that another feature of the MAP pattern includes earlier feedback information, that the next muscle we measure might demonstrate neural feedback, or that extraordinarily rapid reflexes (Holtje and Hustert 2003) are coupled to muscles with extremely rapid force development acting with little delay when played through a viscoelastic mechanical system. However, for dynamic locomotion where bandwidth limitations become important, the more the initial response to perturbation data are explained by mechanical feedback using feed-forward signals, the more the burden of proof shifts to finding a neural, sensory or muscle activation pattern whose change demonstrably affects the dynamics of the whole body in the observed time course of the perturbation and recovery (Holmes et al. 2006).

Kinematic phase data do support neural feedback to the system-level CPG following the perturbation. After a step, the mean residual phase established a new trend (thick dark line, Fig. 4A) with its slope corresponding to an average decrease in frequency by 0.6 Hz from the pre-perturbation values of 11.0 ± 0.2 Hz. The frequency change corresponded to an outcome of the form shown in Fig. 2G, and rejected both purely mechanical feedback (Fig. 1A) and tracking feedback (Fig. 1B) in favor of feedback to the system-level CPG (Fig. 1C). The increase in MAP IBIs of a key leg control muscle (Fig. 7B) paralleled the decrease in residual phase (Fig. 4A) and therefore stride frequency both in magnitude and stride-by-stride timing.

Further supporting evidence for system-level CPG feedback comes from the same species for six of the 150 steps analyzed for rough terrain running (Sponberg and Full 2008). In these few steps, the animal failed to make ground contact during its normal gait cycle, resulting in very large perturbations that presumably drove the animal out of its passive basin of stability. Despite the lack of stance initiation, the rhythmic activation of control muscles persisted for one step, suggesting a continuation of the feed-forward, CPG signal (Fig. 7b, c in Sponberg and Full 2008). Examination of the next stride showed that neural feedback acted to delay stance initiation. During these very large perturbations, the dorsal/ventral femoral extensors did not use sensory information to adjust this muscle within a stride, but acted to shift the phase of the system-level CPG's clock-like signal in the subsequent stride.

Most recently, in middle leg muscles homologous to the control muscle measured in this study, Sponberg et al. (2011a, b) manipulated a freely running animal by reading each neurally produced MAP to trigger additional artificially produced voltage spikes mimicking a modified neural feedback while capturing limb and body dynamics through high-speed videography and a microaccelerometer backpack. Despite changes in timing of the stride where stimulation was introduced, the next stride acted to re-synchronize the alternating tripod such that future strides were indistinguishable from before the added feedback-like signal. This suggested that there was no change to the system-level CPG timing of the alternating tripod gait. Their results are consistent with a system-level CPG acting to establish steady-state running dynamics and neural feedback impinging on these activation patterns below the level where system-level CPG timing occurs.

Our kinematic phase results and MAP recordings during a lateral perturbation of a rapid running animal add to the developing picture of the control of locomotion based on animals in which the dynamics of locomotion play a lesser role (Büschges et al. 2011; Büschges 2005). Büschges et al. [2011] argue that motor signaling in stick insects is generated by neural CPGs (each of which typically generates signaling to a single antagonistic set of muscles) located in a segment proximal to the muscles they control, and whose function is modulated by descending signals. Our results are consistent with this architecture, but we suggest three nested control loops acting at substantially separated time constants (Fig. 1). The outermost, slowest loop involves modulation of the CPGs by descending higher brain centers or high order neural networks. The mid-range loop, reacting at time constants of single strides, interlocks the neural CPGs into a single, somewhat higher system-level CPG. The inner, fastest loop, which handles within-stride stabilization in time constants of a fractional step, is most often implemented mechanically, but does not preclude the possibility of an extremely fast "support reflex" such as been proposed in locust (Holtje and Hustert 2003).

Support for a nested, hierarchical neuromechanical control architecture continues to emerge (Revzen et al. 2008). Fuchs et al. [2011] state for the neural system in cockroaches, "In the absence of sensory feedback, we observed a coordination pattern with consistent phase relationship that shares similarities with a double-tripod gait, suggesting central, feed-forward control." Kukillaya et al. [2009] characterizing the mechanical system conclude that, "the feedforward CPG-driven system is marginally stable, with a weakly stable mode and a neutral mode, making it act as a low-pass filter that yields fairly easily correctable and steerable dynamics."

We hypothesize that the passive mechanical system is sufficiently stable to recover from small perturbations, but not so stable as to obviate the contribution of neural feedback at several levels to recover from large perturbations as delivered in the present experiments.

4.2 Classes of kinematic outcome—effect of leg number and position on lateral stability

Velocity of COM evolved in two different ways depending on pre-perturbation phase leg pose (Fig. 5B, C). The two classes represented statistically significant differences in outcome (Fig. 6), pointing to the power of kinematic phase as a succinct representation of animal state, and thus a predictor of future outcomes. The fact that a phase estimate derived from discrete (PEP) events did not yield a statistically significant kinematic classification in our experiment (Fig. 5G, H) indicates that the increased temporal resolution afforded by instantaneous estimates of kinematic phase provides a more accurate description of an animal's state. From a dynamical systems perspective, the success of phase at predicting future outcomes is not surprising—any stable nonlinear oscillator (such as running animals) can be modeled as a periodic function of phase using Floquet theory (Floquet 1883; Guckenheimer and Holmes 1983), a fact that may make kinematic phase-based methods invaluable to future biomechanical studies.

We hypothesize that the differences in COM velocity and yaw rate between the two outcome classes (Fig. 5B–E) are the consequence of differences in passive mechanical stability with respect to the perturbation. As the cart accelerated to the animals' left, they experienced a force to their right with respect to the cart frame of reference. In C_1 trials, animals were mostly in a left tripod stance with the front left, middle right, and hind left legs on the cart during peak perturbation (Fig. 8, blue). In C_0 trials, animals were in right stance with the front right, middle left and hind right on the cart during peak perturbation (Fig. 8, red). As the animal began to be pulled laterally, the claws of the two feet on its left side could engage the substrate to exert considerable lateral force. For C_0 trials, only the middle leg claws were available on its left side. The animal also experienced a torque when the claws on the middle leg engaged, as the middle leg was typically in front of the center of mass. For C_1 trials, the two sets of claws were located anterior and posterior to the COM. This could allow for a larger lateral force and for the forces to be paired, thus minimizing the torque and facilitating recovery while better preserving orientation and heading. In this manner, animals in the C_1 trials could rely on the mechanical feedback pathway (Fig. 1A) to compensate for a greater part of the perturbation than animals in the C_0 trials, and experienced faster recovery to their final lateral velocity (Vy, Fig. 5C, blue) and more rapid recovery of yaw angle (Fig. 5E, blue).

Kinematic phase allowed us to reduce posture to a univariate time series, so we were able to attribute the difference in perturbation recovery of class C_0 versus C_1 trials to a specific animal pose (Fig. 8). While it is commonly assumed that hexapedal designs are the most stable of legged runners because of their ability to maintain a static stability margin throughout the gait cycle or dynamically move the COM into the next tripod of support (Ting et al. 1994), our results from lateral perturbations expose a limitation of the hexapods' alternating tripod gait. As illustrated in Fig. 8, the C_0 class (red) is constrained in its ability to exert restorative forces and torques, because only one leg is available on that side of the animal's body. We hypothesize that sprawled morphologies with at least two legs in stance on each side of the body will have a significant advantage in recovering from lateral perturbations, and thus may be a useful design target for legged robots. Perhaps animals and robots with eight or more legs would be more robust to lateral perturbations. Initial performance evaluations of a new 8-legged robot (OctoRoaACH) are consistent with these predictions (Pullin et al. 2012).

4.3 Kinematic phase as a tool for neuromechanical and neuroethological studies

We compared the residual from our instantaneous kinematic phase to the residual from phase computed from the timing of posterior extreme positions (PEP) of a selected leg, as commonly used in the biomechanics literature (Cruse et al. 1998; Bender et al. 2010; Maes et al. 2008). Depending on which leg we chose, we observed qualitatively different residual phase outcomes: from no change when using the left front leg (Fig. 9C), to a frequency increase when using the right middle leg (Fig. 9D). Averaging (circular average, Fisher 1993) the PEP phase estimates from all six legs (Fig. 9B) gave a residual phase that most closely resembled our own (Fig. 9A), suggesting that the present method provides a reliable representation of the global phase. We assert that our approach—estimating a phase from the instantaneous state at every sample—resolves true phase (in the dynamical systems sense) much more accurately than methods based on events such as PEP, foot touchdown, EMG IBIs, and other similar events. In those cases where the investigator hypothesizes there to be multiple interacting clocks, such as independent clocks for separate legs, each clock's kinematic phase estimate can be generated from the multiple kinematic measurements that it drives (Revzen et al. 2008), and the coupling between these clocks can then be explored (Kralemann et al. 2007).

Though the phase estimates we derive from PEP events and from instantaneous kinematic data are qualitatively similar (compare Fig. 9A, B), the high temporal resolution intrinsic to instantaneous estimates of phase provide greater insight into the mechanical state of the animal. Specifically, our instantaneous estimate of kinematic phase enabled the identification of a significant difference in kinematic response to a large lateral perturbation based on the mechanical configuration of the animal immediately prior to onset of the perturbation. This result was obscured when using less resolved

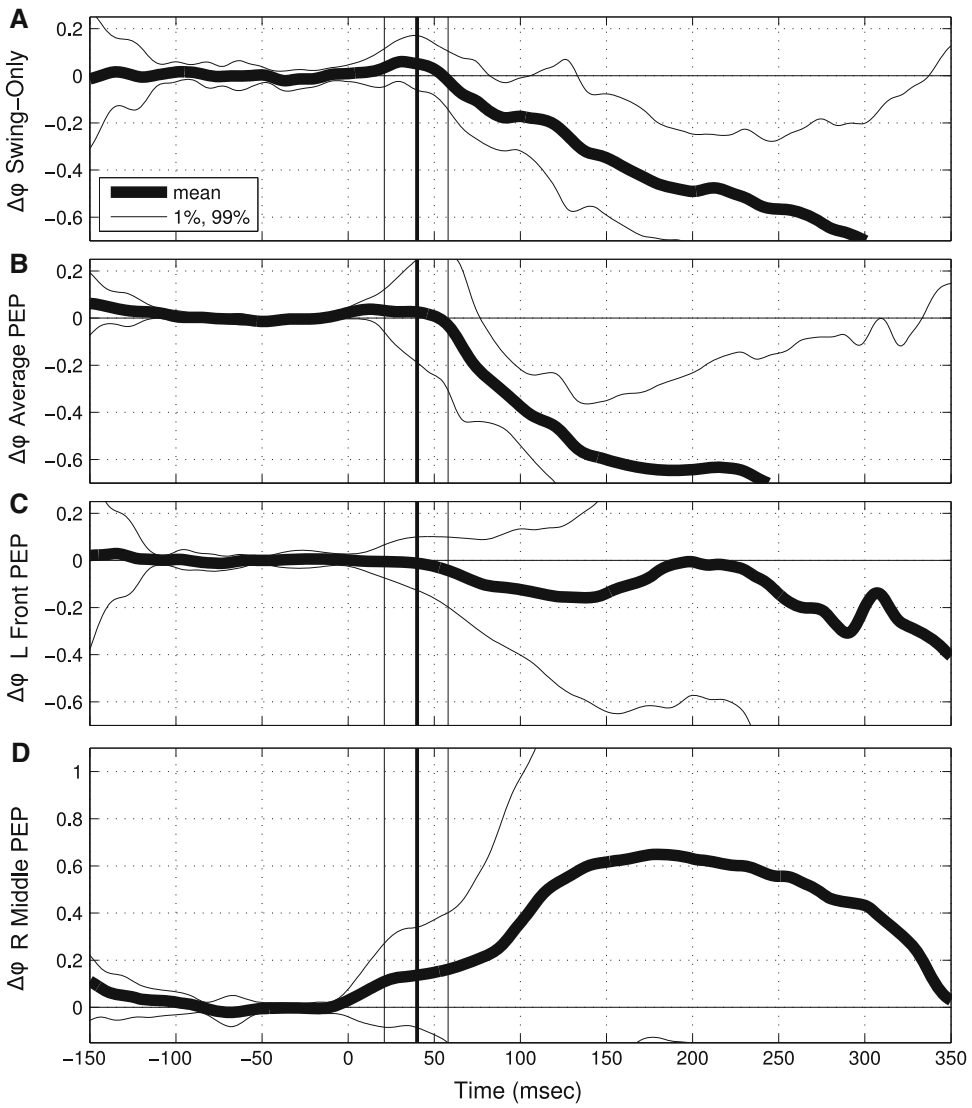

Fig. 9 Comparison of residual phase result from the instantaneous kinematic phase estimation method (**A**) with PEP calculations (**B**–**D**). We plotted the mean of the phase estimate for all trials (*thick black line*, with 1 and 99 % of bootstrap means in *thin black lines*). The vertical thick line at time 0 indicates onset of perturbation. Plots show residual phase obtained from different phase estimation methods: for **A**, we used our instantaneous kinematic phase estimate; in **B**, we estimated phase individually for each leg by taking the transition from stance to swing (PEP) to indicate the start of a new cycle, linearly interpolating between these points and averaging over all 6 legs, to obtain a result similar to **A**; **C** uses the front left leg PEP; **D** uses the right middle leg PEP. **C**, **D** produce results that do not resemble **A** or **B**, nor do they resemble each other

phase estimates derived from discrete events (PEP; compare A–E with F–J in Fig. 5). The capability of revealing kinematic rhythm changes at high temporal resolutions could provide significant benefits to related neuromechanical and neuroethological studies, while providing a convenient proxy for technically difficult neural measurements (Fig. 10). One benefit is that classical analyses such as the "coordination influences" of the WalkNet model of the stick insect *Carausius morosus* (Cruse et al. 1998; Cruse and Schwarze 1988; Cruse and Knauth 1989) can be re-expressed as dynamical models of coupled clocks using quantitative methods for estimation of phase coupling between kinematic phases of legs (Kralemann et al. 2007; Revzen and Guckenheimer 2008), making the generation and analysis of such models a simpler task.

4.4 Dynamical systems bridge bio-inspired simulation and robotics

We found that the delay in appearance of a neurally mediated kinematic response in our system was comparable to at least one stride or step duration. One interpretation of this result

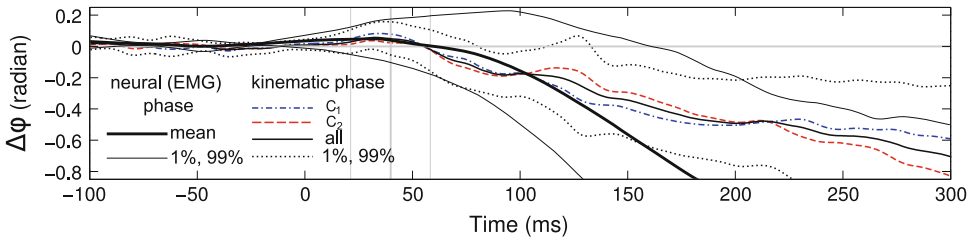

Fig. 10 Plot of residual phase, similar to Fig. 6A, comparing the residual kinematic phase results of Fig. 6A (*dot-dashed* and *dashed colored lines* for the two outcome classes, with a *solid line* between them for the overall mean; *dotted line* for the first and last percentile confidence intervals around the mean), with a residual phase computed from neural (EMG; *thick dark line mean*; *thin solid lines* for the first and last percentile confidence intervals around the mean). We conclude that the neural measurement are consistent with the kinematic phase outcomes, showing the same qualitative structure despite the running speed differences, and failing to reject the better resolved kinematic phase response over the entire duration of measurement

is that neural modulation of gait is applied at step intervals rather than as continuous feedback, expressing a limitation of control ability. Developments in control theory suggest that replacing high rate periodic feedback (which emulates continuous feedback) with control decisions applied at an opportune moment can be an effective strategy, and has the added advantage of decreasing the computational load on the controller (Tabuada 2007; Mazo and Tabuada 2009). We hypothesize that such approaches are particularly beneficial when applied to self-stabilizing systems, such as those that govern cockroach running dynamics, and that the theory of "Self Triggered Control" may prove valuable for the study of gait generation in animals.

In addition, new types of biologically inspired controllers may lead to more effective terrain awareness in legged robots (Spenko et al. 2008; Kim et al. 2006; Webb 2002; Quinn and Ritzmann 1998; Altendorfer et al. 2001; Bachmann et al. 2009). Kinematic phase-based studies are equally applicable to animals, robots, and simulated models. These and other approaches that build on the shared mathematical language of dynamical systems allow for parallel paths of investigation in animal research, robot design, and applied mathematics, to the benefit of all three fields.

Acknowledgments We would like to thank Teressa Alexander for laboratory assistance in collecting EMG data. This work was funded by NSF Frontiers for Integrative Biology Research (FIBR) Grant No. 0425878-Neuromechanical Systems Biology to RJF. SB and JMM were partially supported by NSF Graduate Research Fellowships and an NSF IGERT Traineeship to JMM.

References

Ahn AN, Full RJ (2002) A motor and a brake: two leg extensor muscles acting at the same joint manage energy differently in a running insect. J Exp Biol 205(3):379–389

Ahn AN, Meijer K, Full RJ (2006) In situ muscle power differs without varying in vitro mechanical properties in two insect leg muscles innervated by the same motor neuron. J Exp Biol 209(17), 3370–3382. ISSN 0022-0949. doi:10.1242/jeb.02392

Altendorfer R, Koditschek DE, Holmes P (2004) Stability analysis of legged locomotion models by symmetry-factored return maps. Int J Rob Res. 23(10–11):979–999

Altendorfer R, Moore N, Komsuolu H, Buehler M, Brown HB, McMordie D, Saranli U, Full RJ, Koditschek DE (2001) Rhex: a biologically inspired hexapod runner. Auton Rob 11(3):207–213. ISSN 1573-7527. doi:10.1023/A:1012426720699

Bachmann RJ, Boria FJ, Vaidyanathan R, Ifju PG, Quinn RD (2009) A biologically inspired micro-vehicle capable of aerial and terrestrial locomotion. Mech Mach Theory 44(3):513–526. ISSN 0094-114X doi:10.1016/j.mechmachtheory.2008.08.008

Bender JA, Pollack AJ, Ritzmann RE (2010) Neural activity in the central complex of the insect brain is linked to locomotor changes. Curr Biol 20:921–926

Büschges A (2005) Sensory control and organization of neural networks mediating coordination of multisegmental organs for locomotion. J Neurophysiol 93:1127–1135. doi:10.1152/jn.00615.2004

Büschges A, Scholz H, El-Manira A (2011) New moves in motor control. Curr Biol 21:R513–R524. doi:10.1016/j.cub.2011.05.029

Carbonell C (1947) The thoracic muscles of the cockroach *Periplaneta americana* (L.). Smith Misc Coll 107:1–23

Cruse H, Knauth A (1989) Coupling mechanisms between the contralateral legs of a walking insect (*Carausius morosus*). J Exp Biol 144:199–213

Cruse H, Schwarze W (1988) Mechanisms of coupling between the ipsilateral legs of a walking insect (*Carausius morosus*). J Exp Biol 138:455–469

Cruse H, Durr V, Schmitz J (2007) Insect walking is based on a decentralized architecture revealing a simple and robust controller. Philos Trans R Soc A 365(1850):221–250

Cruse H, Kinderman T, Schumm M, Dean J, Schmitz J (1998) Walknet—a biologically inspired network to control six-legged walking. Neural Netw. 11(7–8):1435–1447

Delcomyn F (1980) Neural basis of rhythmic behavior in animals. Science 210(4469):492–498. doi:10.1126/science.7423199

Dudek DM, Full RJ (2007) An isolated insect leg's passive recovery from dorso-ventral perturbations. J Exp Biol 210:3209–3217. doi:10.1242/jeb.008367

Duysens J, Clarac, Cruse H (2000) Load-regulating mechanisms in gait and posture: comparative aspects. Physiol Rev 80(1):83–133. ISSN 0031-9333. http://physrev.physiology.org/cgi/content/abstract/80/1/83

Fisher NI (1993) Statistical analysis of circular data. Cambridge University Press, Cambridge. ISBN 0-521-35018-2

Floquet G (1883) Sur les Equations différentielles linéaires à coefficients périodiques. Ann Sci Ecole Norm Sup 2:12

Fuchs E, Holmes P, Kiemel T, Ayali A (2011) Intersegmental coordination of cockroach locomotion: adaptive control of centrally coupled pattern generator circuits. Front Neural Circuits 4. doi:10.3389/fncir.2010.00125

Fuchs E, Holmes P, David I, Ayali A (2012) Proprioceptive feedback reinforces centrally generated stepping patterns in the cockroach. J Exp Biol 215:1884–1891. doi:10.1242/jeb.067488

Full RJ, Tu MS (1990) Mechanics of 6-legged runners. J Exp Biol 148:129–146. ISSN 0022-0949

Full RJ, Blickhan R, Ting LH (1991) Leg design in hexapedal runners. J Exp Biol 158:369–390. ISSN 0022-0949

Full RJ, Stokes DR, Ahn A, Josephson RK (1998) Energy absorption during running by leg muscles in a cockroach. J Exp Biol 201: 997–1012

Full RJ, Koditschek DE (1999) Templates and anchors: neuromechanical hypotheses of legged locomotion on land. J Exp Biol 202: 3325–3332

Ghigliazza RM, Altendorfer R, Holmes P, Koditschek DE (2005) A simply stabilized running model. SIAM Rev 47(3):519–549

Grillner S (1972) The role of muscle stiffness in meeting the changing postural and locomotor requirements for force development by the ankle extensors. Acta Physiol Scand 86:92–108

Grillner S (1985) Neurobiological bases of rhythmic motor acts in vertebrates. Science 228:143–149

Grillner S, Wallén P (2002) Cellular bases of a vertebrate locomotor system—steering, intersegmental and segmental co-ordination and sensory control. Brain Res Rev 40(1–3):92–106

Guckenheimer J, Holmes P (1983) Nonlinear oscillations, dynamical systems, and bifurcations of vector fields. Springer, Berlin

Holmes P, Full RJ, Koditschek D, Guckenheimer J (2006) Dynamics of legged locomotion: models, analyses, and challenges. SIAM Rev 48(2):207–304

Holtje M, Hustert R (2003) Rapid mechano-sensory pathways code leg impact and elicit very rapid reflexes in insects. J Exp Biol 206(16):2715–2724. ISSN 0022-0949. doi:10.1242/jeb.00492

Ijspeert AJ (2008) Central pattern generators for locomotion control in animals and robots: a review. Neural Netw. 21(4):642–653. ISSN 0893-6080. doi:10.1016/j.neunet.2008.03.014

Jaric S, Latash ML (2000) The equilibrium-point hypothesis is still doing fine. Hum Mov Sci 19(6):933–938

Jindrich DL, Full RJ (1999) Many-legged maneuverability: dynamics of turning in hexapods. J Exp Biol 202(12):1603–1623

Jindrich DL, Full RJ (2002) Dynamic stabilization of rapid hexapedal locomotion. J Exp Biol 205(18):2803–2823. ISSN 0022-0949

Kalman RE (1960) A new approach to linear filtering and prediction problems. J Basic Eng 82:35–45

Kim S, Clark JE, Cutkosky MR (2006) iSprawl: design and tuning for high-speed autonomous open-loop running. Int J Robot Res 25(9):903–912. ISSN 0278-3649. doi:10.1177/0278364906069150

Klavins E, Komsuoglu H, Full RJ, Koditschek DE (2002) The role of reflexes versus central pattern generators in dynamical legged locomotion. In: Ayers J, Davis J, Rudolph A (eds) Neurotechnology for biomimetic robots. MIT Press, Cambridge, pp 351–382

Kralemann B, Cimponerlu L, Rosenblum M, Pikovsky A, Mrowka R (2007) Uncovering interaction of coupled oscillators from data. Phys Rev E 76(5):055201. ISSN: 1539-3655. doi:10.1103/PhysRevE.76.055201

Kram R, Wong B, Full RJ (1997) Three-dimensional kinematics and limb kinetic energy of running cockroaches. J Exp Biol 200(13):1919–1929. ISSN 0022-0949

Kubow TM, Full RJ (1999) The role of the mechanical system in control: a hypothesis of self-stabilization in hexapedal runners. Phil Trans R Soc B 354(1385):849–861. ISSN 0962-8436

Kukillaya RP, Holmes PJ (2007) A hexapedal jointed-leg model for insect locomotion in the horizontal plane. Biol Cybern 97(5–6): 379–395. ISSN 0340-1200. doi:10.1007/s00422-007-0180-2

Kukillaya RP, Holmes P (2009) A model for insect locomotion in the horizontal plane: feedforward activation of fast muscles, stability, and robustness. J Theor Biol 261(2):210–226. doi:10.1016/j.jtbi.2009.07.036

Kukillaya R, Proctor J, Holmes P (2009) Neuromechanical models for insect locomotion: stability, maneuverability, and proprioceptive feedback. Chaos 19(2). ISSN 1054-1500. doi:10.1063/1.3141306

MacKay-Lyons M (2002) Central pattern generation of locomotion: a review of the evidence. Phys Ther 82(1):69–83. ISSN 0031-9023. http://www.ptjournal.org/cgi/content/abstract/82/1/69

Maes LD, Herbin M, Hackert R, Bels VL, Abourachid A (2008) Steady locomotion in dogs: temporal and associated spatial coordination patterns and the effect of speed. J Exp Biol 211:138–149. doi:10.1242/jeb.008243

Marder E, Bucher D, Schulz D, Taylor A (2005) Invertebrate central pattern generator moves along. Curr Biol 15:685–699

Mazo M, Tabuada P (2009) Input-to-state stability of self-triggered control systems. In: Conference on decision and control, 48th IEEE, pp 928–933

Noah JA, Quimby L, Frazier SF, Zill SN (2004) Walking on a peg leg: extensor muscle activities and sensory feedback after distal leg denervation in cockroaches. J Comp Physiol A 190:217–231. ISSN 0340-7594. doi:10.1007/s00359-003-0488-x

Pearson KG (1993) Common principles of motor control in vertebrates and invertebrates. Ann Rev Neurosci 16:265–297

Pearson KG (1995) Proprioceptive regulation of locomotion. Curr Opin Neurobiol 5:786–791

Pearson KG (2004) Generating the walking gait: role of sensory feedback. Prog Brain Res 143:123–129

Pearson KG, Iles JF (1971) Innervation of coxal depressor muscles in cockroach, *Periplaneta americana*. J Exp Biol 54(1):215–232

Pearson KG, Collins DF (1993) Reversal of the influence of group Ib afferents from plantaris on activity in medial gastrocnemius-muscle during locomotor-activity. J Neurophysiol 70(3):1009–1017. ISSN 0022-3077

Politis DN (1995) A primer on bootstrap methods in statistics. Technical report 95-19. Purdue University. http://www.stat.purdue.edu/research/technical_reports/pdfs/1995/tr95-19.pdf

Politis DN (1998) Computer-intensive methods in statistical analysis. IEEE Signal Proc Mag 15(1):39–55. ISSN 1053-5888. doi:10.1109/79.647042

Prochazka A, Gillard D, Bennett DJ (1997a) Implications of positive feedback in the control of movement. J Neurophysiol 77(6):3237–3251. ISSN 0022-3077

Prochazka A, Gillard, D, Bennett DJ (1997b) Positive force feedback control of muscles. J Neurophysiol 77(6):3226–3236. ISSN 0022-3077

Proctor J, Holmes PJ (2008) Steering by transient destabilization in piecewise-holonomic models of legged locomotion. Regul Chaotic Dyn 13(4):267–282. doi:10.1134/S1560354708040047

Proctor J, Holmes PJ (2010) Reflexes and preflexes: on the role of sensory feedback on rhythmic patterns in insect locomotion. Biol Cybern 102:513–531. doi:10.1007/s00422-010-0383-9

Proctor J, Kukillaya RP, Holmes P (2010) A phase-reduced neuromechanical model for insect locomotion: feed-forward stability and proprioceptive feedback. Phil Trans R Soc A 368:5087–5104

Pullin AO, Kohut NJ, Zarrouk D, Fearing RS (2012) Dynamic turning of 13 cm robot comparing tail and differential drive. In: IEEE international conference on robotics and automation, May

Quinn RD, Ritzmann RE (1998) Construction of a hexapod robot with cockroach kinematics benefits both robotics and biology. Connect Sci 10(3–4):239–254. ISSN 0954-0091. doi:10.1080/095400998116422

Rauch HE, Tung F, Striebel CT (1965) Maximum likelihood estimates of linear dynamic systems. AIAA J 3(8):1445–1450. ISSN 0001-1452

Revzen S (2009) Neuromechanical control architectures of arthropod locomotion. PhD Thesis. University of California, Berkeley

Revzen S, Guckenheimer JM (2008) Estimating the phase of synchronized oscillators. Phys Rev E 78(5):051907. ISSN 1539-3755. doi:10.1103/PhysRevE.78.051907

Revzen S, Koditschek DE, Full RJ (2008) Towards testable neuromechanical control architectures for running. In: Sternad D (ed) Progress in motor control—a multidisciplinary perspective, pp 25–56. Springer, New York doi:10.1007/978-0-387-77064-2-3

Ridgel AL, Ritzmann RE (2005) Effects of neck and circumoesophageal connective lesions on posture and locomotion in the cockroach. J Comp Physiol A 191(6):559–573

Ridgel A, Frazier F, Zill SN (2001) Dynamic responses of tibial campaniform sensilla studied by substrate displacement in freely moving cockroaches. J Comp Physiol A 187(5):405–420. doi:10.1007/s003590100213

Ritzmann RE, Büschges A (2007) Adaptive motor behavior in insects. Curr Opin Neurobiol 17(6):629–636. ISSN 0959-4388. doi:10.1016/j.conb.2008.01.001

Schilling M, Cruse H, Arena P (2007) Hexapod walking: an expansion to walknet dealing with leg amputations and force oscillations. Biol Cybern 96(3):323–340. ISSN 0340-1200. doi:10.1007/s00422-006-0117-1

Schmitt J, Holmes P (2000a) Mechanical models for insect locomotion: dynamics and stability in the horizontal plane I. Theory. Biol Cybern 83(6):501–515

Schmitt J, Holmes P (2000b) Mechanical models for insect locomotion: dynamics and stability in the horizontal plane II. Application. Biol Cybern 83(6):517–527

Schmitt J, Holmes P (2001) Mechanical models for insect locomotion: stability and parameter studies. Physica D 156(1–2):139–168

Schmitt J, Holmes P (2003) Mechanical models for insect locomotion: active muscles and energy losses. Biol Cybern 89(1): 43–55. ISSN 0340-1200. doi:10.1007/s00422-003-0404-z

Schmitt J, Garcia M, Razo RC, Holmes P, Full RJ (2002) Dynamics and stability of legged locomotion in the horizontal plane: a test case using insects. Biol Cybern 86(5):343–353

Seyfarth A, Geyer H, Herr H (2003) Swing-leg retraction: a simple control model for stable running. J Exp Biol 206(15):2547–2555

Spagna JC, Goldman DI, Lin P-C, Koditschek DE, Full RJ (2007) Distributed mechanical feedback in arthropods and robots simplifies control of rapid running on challenging terrain. Bioinspir Biomim 2(1): 9–18. ISSN 1748-3182. doi:10.1088/1748-3182/2/1/002

Spenko MJ, Haynes GC, Saunders JA, Cutkosky MR, Rizzi AA, Full RJ, Koditschek DE (2008) Biologically inspired climbing with a hexapedal robot. J Field Robot 25(4–5):223–242. ISSN 1556-4959. doi:10.1002/rob.20238

Spence AJ, Revzen S, Seipel J, Mullens C, Full RJ (2010) Insects running on elastic surfaces. J Exp Biol 213:1907–1920. ISSN 0022-0949. doi:10.1242/jeb.042515

Sponberg S, Full RJ (2008) Neuromechanical response of musculoskeletal structures in cockroaches during rapid running on rough terrain. J Exp Biol 211(3):433–446. ISSN 0022-0949. doi:10.1242/jeb.012385

Sponberg S, Libby T, Mullens C, Full RJ (2011a) Shifts in a single muscle's control potential of body dynamics. Phil Trans R Soc B 366:1606–1620. doi:10.1098/rstb.2010.0368

Sponberg S, Spence A, Mullens C, Full RJ (2011b) A single muscle's multifunctional control potential of body dynamics for postural control and running. Philos Trans R Soc B 366:1592–1605. doi:10.1098/rstb.2010.0367

Tabuada P (2007) Event-triggered real-time scheduling of stabilizing control tasks. IEEE Trans Autom Control 52(9):1680–1685. ISSN 0018-9286. doi:10.1109/TAC.2007.904277

Ting LH, Blickhan R, Full RJ (1994) Dynamic and static stability in hexapedal runners. J Exp Biol 197:251–269. ISSN 0022-0949

Watson JT, Ritzmann RE (1998a) Leg kinematics and muscle activity during treadmill running in the cockroach, *Blaberus discoidalis*: I. Slow running. J Comp Physiol A 182(1):11–22. ISSN 0340-7594. doi:10.1007/s003590050153

Watson JT, Ritzmann RE (1998b) Leg kinematics and muscle activity during treadmill running in the cockroach, *Blaberus discoidalis*: II. Fast running. J Comp Physiol A 182(1):23–33. ISSN 0340–7594. doi:10.1007/s003590050154

Watson JT, Ritzmann RE, Pollack AJ (2002a) Control of climbing behavior in the cockroach, *Blaberus discoidalis*. II. Motor activities associated with joint movement. J Comp Physiol A 188(1):55–69. ISSN 0340-7594. doi:10.1007/s00359-002-0278-x

Watson JT, Ritzmann RE, Zill SN, Pollack AJ (2002b) Control of obstacle climbing in the cockroach, Blaberus discoidalis. I. Kinematics. J Comp Physiol A 188(1):39–53. ISSN 0340-7594. doi:10.1007/s00359-002-0277-y

Webb B (2002) Robots in invertebrate neuroscience. Nature 417(6886):359–363. ISSN 0028-0836

Wilson DM (1961) The central nervous control of flight in a locust. J Exp Biol 38:471–490

Zehr EP, Stein RB (1999) What functions do reflexes serve during human locomotion? Prog Neurobiol 58(2):185–205. ISSN 0301–0082

Zill SN, Moran DT, Varela, FG (1981) The exoskeleton and insect proprioception. 2. Reflex effects of tibial campaniform sensilla in the american cockroach, *Periplaneta americana*. J Exp Biol 94:43–55. ISSN 0022-0949

Zill SN, Schmitz J, Büschges A (2004) Load sensing and control of posture and locomotion. Arthropod Struct Dev 33(3):273–286. ISSN 1467-8039. doi:10.1016/j.asd.2004.05.005

Zill SN Keller BR, Duke ER (2009) Sensory signals of unloading in one leg follow stance onset in another leg: transfer of load and emergent coordination in cockroach walking. J Neurophysiol 101(5):2297–2304. ISSN 0022-3077. doi:10.1152/jn.00056.2009